

NONLINEAR ANALYSIS OF MOORING LINES
AND MARINE RISERS

HUI YIN





Library and
Archives Canada

Bibliothèque et
Archives Canada

Published Heritage
Branch

Direction du
Patrimoine de l'édition

395 Wellington Street
Ottawa ON K1A 0N4
Canada

395, rue Wellington
Ottawa ON K1A 0N4
Canada

Your file *Votre référence*
ISBN: 978-0-494-33457-7
Our file *Notre référence*
ISBN: 978-0-494-33457-7

NOTICE:

The author has granted a non-exclusive license allowing Library and Archives Canada to reproduce, publish, archive, preserve, conserve, communicate to the public by telecommunication or on the Internet, loan, distribute and sell theses worldwide, for commercial or non-commercial purposes, in microform, paper, electronic and/or any other formats.

The author retains copyright ownership and moral rights in this thesis. Neither the thesis nor substantial extracts from it may be printed or otherwise reproduced without the author's permission.

AVIS:

L'auteur a accordé une licence non exclusive permettant à la Bibliothèque et Archives Canada de reproduire, publier, archiver, sauvegarder, conserver, transmettre au public par télécommunication ou par l'Internet, prêter, distribuer et vendre des thèses partout dans le monde, à des fins commerciales ou autres, sur support microforme, papier, électronique et/ou autres formats.

L'auteur conserve la propriété du droit d'auteur et des droits moraux qui protègent cette thèse. Ni la thèse ni des extraits substantiels de celle-ci ne doivent être imprimés ou autrement reproduits sans son autorisation.

In compliance with the Canadian Privacy Act some supporting forms may have been removed from this thesis.

Conformément à la loi canadienne sur la protection de la vie privée, quelques formulaires secondaires ont été enlevés de cette thèse.

While these forms may be included in the document page count, their removal does not represent any loss of content from the thesis.

Bien que ces formulaires aient inclus dans la pagination, il n'y aura aucun contenu manquant.


Canada

**Nonlinear Analysis
of Mooring Lines and Marine Risers**

by

©Hui Yin
St. John's, Newfoundland, Canada

B.Eng., Shanghai Jiaotong University, China (1991)
M.Eng., Tsinghua University, China (1996)

A thesis submitted to the
School of Graduate Studies
in partial fulfillment of the
requirements for the degree of
Master of Engineering

Faculty of Engineering and Applied Science
Memorial University of Newfoundland

July 2007

Nonlinear Analysis of Mooring Lines and Marine Risers

by

Hui Yin

St. John's, Newfoundland, Canada

Abstract

A six degree-of-freedom finite element numerical code, named MAPS-Mooring, has been developed for the static and dynamic analysis of mooring lines and marine risers. The three dimensional global-coordinate-based finite element method is adopted to model the mooring lines. In this method, the global coordinate system is used to describe the position of mooring lines instead of introducing local coordinate systems. The geometric nonlinearity and the environmental load nonlinearity are considered. Assuming that the sea bottom is flat and elastic, the non-penetrating bottom boundary conditions are applied on the sea floor in the analysis.

In the computation, the static problem is first solved to determine the initial profile of mooring lines. When solving the static problem, the inertia term is neglected. The governing differential equations of the mooring line are a set of nonlinear algebraic equations which are solved by Newton's iteration method. For dynamic problems, the first-order differential equations are solved by the first-order Adams-Moulton method.

The developed program was verified and validated by its applications to various

mooring systems and marine risers. The reliability and accuracy of the program has been demonstrated by comparing the numerical solutions with the analytical solutions, experimental data and numerical results by other programs.

Acknowledgements

I would like to express my gratitude to Dr. Wei Qiu, my supervisor, for his encouragement, guidance and support throughout this research and the daily life.

I would like to give my deep appreciation to the support of the Mathematics of Information Technology and Complex Systems (MITACS) and Oceanic Consulting Corporation through a MITACS Internship Program. This work was also supported by the Natural Sciences and Engineering Research Council of Canada (NSERC). Without the NSERC support, this work could never be possibly completed. I would like also to thank the support of Graduate Study Fellowship of Memorial University of Newfoundland.

Finally, I am grateful to my family and my mother-in-law who were always there to encourage and support me throughout my studies and research.

Contents

Acknowledgements	iii
Abstract	v
List of Figures	vii
List of Tables	vii
Nomenclature	xi
1 Introduction	1
1.1 Background	1
1.2 Literature Review	2
1.3 Thesis Contents	5
2 Mathematical Formulation of the Global-Coordinate-Based Finite Element Method	6
2.1 Equations of Motion of A Slender Rod	7
2.2 Finite Element Modeling	12
2.3 Formulation for Static Problem	16
2.4 Formulation for Dynamic Problem - Time Domain Integration	19
2.5 The Sea Bottom Boundary Condition	24

3 Numerical Results	26
3.1 Simple Catenary Mooring Line	26
3.2 Moored Surface Buoy Under Steady Current	28
3.3 Multiple Mooring Lines System	30
3.4 Large-Amplitude Motion of A Rigid Pendulum	33
3.5 Validation Studies for Dynamic Analysis	35
3.6 Vortex Induced Vibration of Marine Riser	40
4 Conclusions and Recommendations	45
References	47

List of Figures

2-1	Coordinate System of Mooring Line	7
2-2	Sea Bottom Boundary Condition	24
3-1	Simple Catenary Mooring Line	27
3-2	Moored Surface Buoy Under Steady Current	29
3-3	Equilibrium Position of Mooring Line under Steady Current	29
3-4	Plan View of the Mooring System (Brown and Lyons, 1998)	30
3-5	Three Dimensional Configuration of the Mooring System	31
3-6	Comparison of Results by MAPS-Mooring, MOOR and Mooring-System	33
3-7	Initial Position of the Uniform Rigid Bar	34
3-8	Motion of Uniform Rigid Bar	34
3-9	Sensitivity to Number of Elements	36
3-10	Sensitivity to Time Step	37
3-11	Time-domain Tension at Nondimensional Motion Amplitude of 0.03 .	37
3-12	Time-domain Tension at Nondimensional Motion Amplitude of 0.065	38
3-13	Time-domain Tension at Nondimensional Motion Amplitude of 0.075	38
3-14	Time-domain Tension at Nondimensional Motion Amplitude of 0.095	39
3-15	Nondimensional Dynamic Line Tension	39
3-16	Lift Coefficient Plot	41
3-17	Rigid Riser Model	42
3-18	Cross-flow Motion of the Riser ($U=1.65\text{m/s}$)	43
3-19	Cross-flow Motion of the Riser ($U=1.8\text{m/s}$)	44

List of Tables

3.1	Catenary - Comparison between Numerical Solutions and Analytical Results	28
3.2	Coordinates of Fairleads and Azimuth Angles of the Mooring Lines .	32
3.3	Characteristics of the Mooring Line Used in the Analysis and Experiments	35
3.4	Comparison of Numerical Solutions and Experimental Results	43

Nomenclature

A	cross-sectional area
A_k	interpolation function
B	buoyancy force per unit length
C_A	added mass coefficient
C_D	drag coefficient
C_M	inertial coefficient
C_V	tolerance of tangential velocity
E	elastic modulus of the material
F	resultant force
F^d	hydrodynamic force per unit length
F^s	hydrostatic force per unit length
H	torque
I	moment of inertia of the cross section
L	length of an element
M	resultant moment

P_m	interpolation function
P_s	hydrostatic pressure
R	distance from the centerline of the mooring line to the outer most fiber of the mooring line
T	tension
$T_{dynamic}$	dynamic tension
T_{nondim}	nondimensional line tension
T_{static}	static tension
\tilde{T}	effective tension
U_{ik}	coefficients in the interpolation function
\mathbf{V}	total water particle velocity
V_t	tangential velocity of the mooring line
\mathbf{V}_{rel}^n	relative fluid velocity normal to the centerline of the mooring line
$\dot{\mathbf{V}}$	total water particle acceleration
$\dot{\mathbf{V}}^n$	acceleration normal to the centerline of the mooring line
Z_{bottom}	z coordinate of the sea floor
a	amplitude of fairlead motion
d	water depth
g	gravitational acceleration
\mathbf{m}	applied moment per unit length

\mathbf{q}	applied force per unit length
q^{spring}	distributed spring coefficient
\mathbf{r}	position vector of mooring lines
\mathbf{r}_i	component of \mathbf{r} in i th direction
$\dot{\mathbf{r}}$	velocity of mooring line
$\dot{\mathbf{r}}^n$	velocity of mooring line normal to its centerline
$\ddot{\mathbf{r}}$	acceleration of mooring line
$\ddot{\mathbf{r}}^n$	component of acceleration of mooring line normal to its centerline
\mathbf{r}'	unit tangent vector
\mathbf{r}''	principal normal vector
s	arc length of mooring line measured along the centerline
t	time
\mathbf{w}	weight of the rod per unit length
$\tilde{\mathbf{w}}$	effective weight
κ	curvature of the line
λ	Lagrangian multiplier
λ_m	coefficients in the interpolation function
μ_f	dynamic bottom friction coefficient
ρ	mass per unit length
ξ	nondimensional length

δ_{ij} Kronecker Delta function

Chapter 1

Introduction

1.1 Background

With the oil and gas development in deep water, floating offshore structures are becoming increasingly important. Typical floating offshore structures include Spars, Floating Production Storage and Offloading (FPSO) systems, Semi-submersibles, Tension Leg Platforms (TLPs). These floating structures are usually kept in station by mooring and/or tendon systems. To ensure the normal drilling and/or production activities, the offset of a floating platform should be limited. It is important to predict the load and motion characteristics of a floating platform in the design process.

Moored floating structures are different from both fixed offshore structures and ships in terms of the load and motion characteristics. In ship-motion problems, first-order theory can give reasonable predictions for moderate seas. For moored offshore platforms, second-order responses are of great importance. Normally, floating offshore structures, such as Spars and TLPs, are designed so that their natural frequencies are away from the dominant wave frequency in order to avoid possible large responses at wave frequencies. However, this makes their natural frequencies close to the second-order wave frequencies, i.e., difference-frequencies and/or sum-frequencies. Although the magnitudes of the second-order waves are in general small, they may be of primary

concern in the mooring system design when their frequencies are close to the natural frequencies of the platform motions and when the corresponding damping forces are small. Typical examples are the low-frequency motions in the horizontal plane of Spars and high-frequency motions in the vertical plane of TLPs. And the second-order forces may cause significant increase in mooring line tension and horizontal offset.

The dynamic characteristics of mooring lines significantly affect the motion characteristics of moored floating structures, especially in deep water. For deep water platforms, the length of mooring lines and risers cannot be scaled due to the depth limitation of existing wave basins and the experimental methods cannot be reliably employed for design verification. Under these circumstances, the development of numerical tools for mooring line analysis is essential for the prediction of the dynamic characteristics of mooring lines and motion characteristics of floating structures.

1.2 Literature Review

The topology of a mooring line can be quite simple. However, the very simple system can be the most difficult to model. The challenges in the analysis of mooring lines are associated with the nonlinearities listed below:

- Geometric nonlinearity - the geometric nonlinearity is associated with the changes in shape of the mooring line. Being flexible and lacking a redundant load path, the mooring line can resist imposed loads only by changing its position.
- Nonlinear bottom boundary condition - some portion of the mooring line is usually in contact with the sea floor. The length of the grounded line constantly changes due to the second-order slowly varying motion of the floating structure. This also causes an interaction between the bottom boundary nonlinearity and the geometric nonlinearity.

- Nonlinear hydrodynamic load - The drag force on the mooring line is proportional to the square of the relative velocity between the mooring line and fluid.

There are numerous literatures regarding the dynamics of mooring line. Migliore *et al.* (1979, 1982) and Triantafyllou (1984, 1987, 1991, 1992) reviewed the methods used in dynamic mooring line analysis. More recently, Kamman and Huston (2001) developed multibody dynamics model for variable length cable system. The most commonly used models are listed as below:

- A. Simple massless spring - This is normally used in the situations where the effect of a static restoring force is needed and dynamics or spatial variations of the load in the mooring line can be neglected (Jain, 1980). This method is employed in the first-order analysis of floating structures and it is not appropriate for the computation of the second-order effect of the moored floating structures.
- B. Catenaries - The well-known catenary equations can be used to model the mooring line (Berteaux, 1976; Patel *et al.*, 1994). This method can give good results in some situations, but it is difficult to model a complicated mooring system with multiple lines and with multiple segments with different cross-sectional properties.
- C. Lumped parameter model - This model treats the mooring line as a collection of lumped masses at nodes which are connected by massless straight springs (Nakajima, 1986; Khan *et al.*, 1986; and Ansari, 1986). The external loads are lumped at the same finite number of nodes. The equations of equilibrium and continuity are developed on these nodes. The equations can be solved by the finite difference method (Huang, 1994). This approach is roughly equivalent to the finite element method with straight line elements (truss elements or 1-D simplex elements). Typical implementations of this approach are inferior to the finite element method in terms of computational flexibility and accuracy (Paulling and Webster, 1986).

D. Finite element method (FEM) - This is the most general modeling tool for mooring lines (Malahy, 1986). The finite element method employs interpolation functions to describe the behavior of a given variable within an element in terms of a set of generalized coordinates. The interpolation function defines the relationship between the generalized coordinates and the displacement at any point on the element. Applying the interpolation function to the kinematic equations, constitutive equations and the equilibrium equations, the equations of motion for a single element can be obtained. By assembling the equations for each element and introducing the boundary conditions, the equations of motion for the whole system can be obtained. The finite element method can offer a variety of element forms and it can model complicated mooring systems. Truss or beam elements can be used in the finite element method to model mooring lines (Hwang, 1986, Wu, 1993), which allow variation of fluid loads over its length. The total Lagrangian or updated Lagrangian formulations can be utilized to consider the geometric nonlinearity (Bathe, 1996).

Nordgren (1974) formulated the nonlinear equations of motion based on theory of rod for the three-dimensional inextensible elastic rods with equal principal stiffness and solved them by the finite difference method. Garrett (1982) used the same equations and solved them by a finite element method, which increased the degrees of freedom by introducing a Lagrange multiplier which has the purpose of realizing the inextensibility condition. In the work of Garrett (1982), only a global coordinate system was used. Since there is no local coordinate system introduced, there are no computations of coordinate transformation. Paulling and Webster (1986) further extended this method to allow for small elongation of the rod. Large deflection, bending stiffness and tension variation along its length were considered in this method.

The global-coordinate-based, nonlinear FEM can fully take advantage of the slenderness of mooring lines. In this research, this method will be employed.

1.3 Thesis Contents

The goal of this research is to develop numerical tools to predict the nonlinear dynamic characteristics of mooring lines and marine risers. Similar to mooring lines, risers introduce hydrodynamic forces to the system and provide some restoring forces and damping forces. For simplicity, we will use mooring lines to represent both mooring lines and risers hereafter. Due to the nonlinearities of the mooring system, the dynamic analysis of mooring lines will be conducted in the time domain. The scope of this thesis include the development of the numerical method for static and dynamic analysis of mooring lines.

In this thesis, the derivation of the equations of motion of a slender rod is presented in Chapter 2. The development of the equations of motion and the mathematical formulations of the static and dynamic problem are discussed in detail. Chapter 3 describes the numerical results of various mooring systems and marine risers computed by the developed program based on the mathematical formulations in Chapter 2. The numerical solutions were compared with the analytical solutions and experimental results. Conclusions are drawn in Chapter 4. Recommendations are also given for future research.

Chapter 2

Mathematical Formulation of the Global-Coordinate-Based Finite Element Method

In this chapter, the statics and the dynamics of mooring lines and its numerical implementation are addressed. In the mooring analysis, the static analysis is typically conducted first to determine the static equilibrium position and the static tension of mooring lines. The dynamic analysis of the mooring lines is then carried out based on the static analysis results. Due to the nonlinear geometrical characteristics of mooring lines and complexity of the loads, a robust method is required to predict the motion and tension of the mooring lines. The global-coordinate-based, nonlinear finite element method (FEM) (Garrett, 1982; Paulling and Webster, 1986; and Ran, 2000) is applied in this research.

Considering large deflection, bending stiffness and tension variation along the mooring line, the equations of motion of the mooring are first developed based on the theory of rod. The discretized form of equations of motion are then obtained by applying Galerkin's method. When solving the static problem, the inertia term is neglected. The governing differential equations of the mooring line are a set of

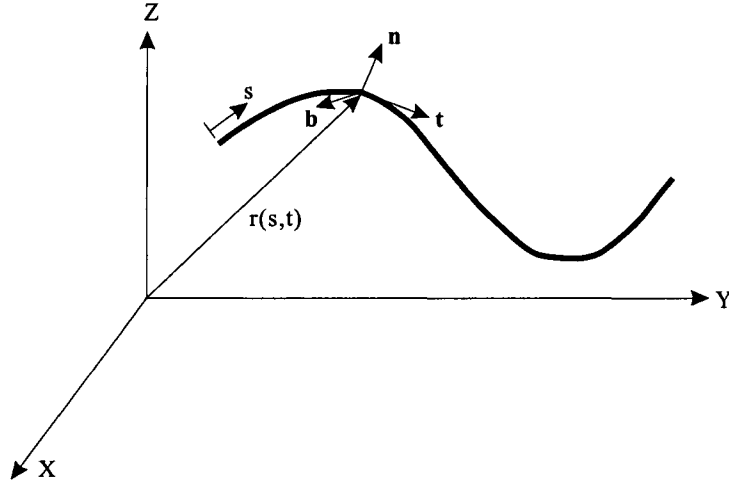


Figure 2-1: Coordinate System of Mooring Line

nonlinear algebraic equations which are solved by Newton's iteration method. For dynamic problems, the second-order differential equations are substituted by a set of first-order differential equations. The first-order Adams-Moulton method is used to integrate the equations.

2.1 Equations of Motion of A Slender Rod

A 3-D Cartesian coordinate system is employed in which the xy plane coincides with the calm water surface and z -axis is upward positive. As shown in Figure 2-1, the position of a segment of mooring line can be defined by the position vector $\mathbf{r}(s,t)$ which is the function of time, t , and the arc length, s , measured along the centerline of the mooring line.

Introducing the unit tangent vector, $\mathbf{r}' = \frac{d\mathbf{r}}{ds}$, and the principal normal vector, $\mathbf{r}'' = \frac{d^2\mathbf{r}}{ds^2}$, the bi-normal vector is directed along $\mathbf{r}' \times \mathbf{r}''$. The mooring line can be considered as a slender rod. For a segment of rod with unit arc length, we can have the following equations of motion based on the momentum conservation:

$$\mathbf{F}' + \mathbf{q} = \rho \ddot{\mathbf{r}} \quad (2.1)$$

$$\mathbf{M}' + \mathbf{r}' \times \mathbf{F} + \mathbf{m} = \mathbf{0} \quad (2.2)$$

where \mathbf{F} is the resultant force, \mathbf{M} is the resultant moment at a point on the rod acting along the centerline, \mathbf{q} is the applied force per unit length, ρ is the mass per unit length of the rod, \mathbf{m} is the applied moment per unit length, the superposed dot denotes the time derivative and the prime denotes the partial derivative with respect to arc length s .

For an elastic rod with equal principal stiffness, the bending moment is proportional to curvature and is directed along the binormal vector. Thus the resultant moment can be written as

$$\mathbf{M} = \mathbf{r}' \times E I \mathbf{r}'' + H \mathbf{r}' \quad (2.3)$$

where E is the elastic modulus of the material of the rod, I is the moment of inertia of the cross section of the rod, and H is the torque. Substituting Equation (2.3) into Equation (2.2) yields

$$(\mathbf{r}' \times E I \mathbf{r}'' + H \mathbf{r}')' + \mathbf{r}' \times \mathbf{F} + \mathbf{m} = \mathbf{0} \quad (2.4)$$

$$\mathbf{r}' \times (E I \mathbf{r}'')' + \mathbf{r}'' \times E I \mathbf{r}'' + H' \mathbf{r}' + H \mathbf{r}'' + \mathbf{r}' \times \mathbf{F} + \mathbf{m} = \mathbf{0} \quad (2.5)$$

With $\mathbf{r}'' \times E I \mathbf{r}'' = 0$, we can obtain

$$\mathbf{r}' \times [(E I \mathbf{r}'')' + \mathbf{F}] + H' \mathbf{r}' + H \mathbf{r}'' + \mathbf{m} = \mathbf{0} \quad (2.6)$$

Taking dot product of Equation (2.6) by \mathbf{r}' yields

$$\mathbf{r}' \cdot \mathbf{r}' \times [(E I \mathbf{r}'')' + \mathbf{F}] + \mathbf{r}' \cdot H' \mathbf{r}' + \mathbf{r}' \cdot H \mathbf{r}'' + \mathbf{r}' \cdot \mathbf{m} = 0 \quad (2.7)$$

Note that $\mathbf{r}' \cdot \mathbf{r}' \times [(E I \mathbf{r}'')' + \mathbf{F}] = 0$, $\mathbf{r}' \cdot \mathbf{r}' \times [(E I \mathbf{r}'')' + \mathbf{F}] = 0$, $\mathbf{r}' \cdot H \mathbf{r}'' = 0$ and

$\mathbf{r}' \cdot \mathbf{r}' = 1$, Equation (2.7) can be written as

$$H' + \mathbf{m} \cdot \mathbf{r}' = 0 \quad (2.8)$$

If there is no distributed torsional moment $\mathbf{m} \cdot \mathbf{r}'$, it is shown in Equation (2.8) that the torque H is independent of arc length s . It is assumed that mooring lines have circular cross sections, and therefore there is no distributed torsional motion and torsional moment from the hydrodynamic forces. In addition, the torque in the lines is usually negligible. In this case, both \mathbf{H} and \mathbf{m} are zero. Equation (2.6) can be simplified as:

$$\mathbf{r}' \times [(EI\mathbf{r}'')' + \mathbf{F}] = \mathbf{0} \quad (2.9)$$

Equation (2.9) shows that the vector, $(EI\mathbf{r}'')' + \mathbf{F}$, is parallel to the centerline of the rod. Introducing a scalar function $\lambda(s, t)$ leads to:

$$(EI\mathbf{r}'')' + \mathbf{F} = \lambda\mathbf{r}' \quad (2.10)$$

$$\mathbf{F} = -(EI\mathbf{r}'')' + \lambda\mathbf{r}' \quad (2.11)$$

Taking dot product by \mathbf{r}' to the above equation yields:

$$\lambda = \mathbf{F} \cdot \mathbf{r}' + (EI\mathbf{r}'')' \cdot \mathbf{r}' \quad (2.12)$$

Using $\mathbf{r}' \cdot \mathbf{r}''' = (\mathbf{r}' \cdot \mathbf{r}'')' - \mathbf{r}'' \cdot \mathbf{r}'' = 0 - \kappa^2 = -\kappa^2$, we have

$$\lambda = T - EI\kappa^2 \quad (2.13)$$

where T is the tension of the rod and κ is the curvature of the line. Combining Equations (2.1) and (2.11) yields the equation of motion for the rod as follows:

$$-(EI\mathbf{r}'')'' + (\lambda\mathbf{r}')' + \mathbf{q} = \rho\ddot{\mathbf{r}} \quad (2.14)$$

In addition, \mathbf{r} must satisfy the inextensibility condition:

$$\mathbf{r}' \cdot \mathbf{r}' = 1 \quad (2.15)$$

If the rod is considered stretchable and the stretch is linear and small, the above inextensibility condition can be approximated by:

$$\mathbf{r}' \cdot \mathbf{r}' = (1 + \epsilon)^2 \approx 1 + 2\epsilon = 1 + 2\frac{T}{AE} \quad (2.16)$$

or

$$\frac{1}{2}(\mathbf{r}' \cdot \mathbf{r}' - 1) = \frac{T}{AE} \approx \frac{\lambda}{AE} \quad (2.17)$$

where the scalar function λ is the Lagrangian multiplier, ϵ is the strain, A is the cross section area of the mooring line, E is again the elastic modulus. The dependent variables, $\mathbf{r}(s, t)$ and $\lambda(s, t)$, can be solved from Equations (2.14), (2.15) or (2.17) in combination with the initial conditions and the boundary conditions. The applied force \mathbf{q} on the mooring lines includes the hydrostatic and hydrodynamic force from surrounding fluid, and the gravity force of the rod, i.e.,

$$\mathbf{q} = \mathbf{w} + \mathbf{F}^s + \mathbf{F}^d \quad (2.18)$$

where \mathbf{w} , \mathbf{F}^s , \mathbf{F}^d are the weight of the rod per unit length, the hydrostatic force per unit length and the hydrodynamic force per unit length, respectively.

The hydrostatic force can be written as:

$$\mathbf{F}^s = \mathbf{B} + (P_s A \mathbf{r}')' \quad (2.19)$$

where \mathbf{B} is the buoyancy force on the rod per unit length (assuming the cross sections are subjected to the hydrostatic pressure), and P_s is the hydrostatic pressure at the point \mathbf{r} on the rod. The second term $(P_s A \mathbf{r}')'$ is due to the pressure difference between .

the two ends. Note that the two ends of the segment are not exposed to the fluid, therefore the pressure force on the ends needs to be deducted from the buoyancy force. The hydrodynamic force on the rod can be obtained from Morrison's equation:

$$\begin{aligned}\mathbf{F}^d &= -C_A\ddot{\mathbf{r}}^n + C_M\dot{\mathbf{V}}^n + C_D|\mathbf{V}_{rel}^n|\mathbf{V}_{rel}^n \\ &= -C_A\ddot{\mathbf{r}}^n + \tilde{\mathbf{F}}^d\end{aligned}\quad (2.20)$$

where C_A is the added mass per unit length, C_M is the inertia force per unit length per unit normal acceleration, and C_D is the drag force per unit length per unit normal velocity. In Equation (2.20), \mathbf{V}_{rel}^n and $\dot{\mathbf{V}}^n$ are the fluid velocity and acceleration normal to the centerline of the rod, respectively. Assuming that the fluid field is not disturbed by the existence of the rod, they can be obtained from the total fluid velocity and the tangent vector of the line:

$$\mathbf{V}_{rel}^n = (\mathbf{V} - \dot{\mathbf{r}}) - [(\mathbf{V} - \dot{\mathbf{r}}) \cdot \mathbf{r}'] \cdot \mathbf{r}' \quad (2.21)$$

$$\dot{\mathbf{V}}^n = \dot{\mathbf{V}} - (\dot{\mathbf{V}} \cdot \mathbf{r}') \cdot \mathbf{r}' \quad (2.22)$$

where \mathbf{V} and $\dot{\mathbf{V}}$ are the total water particle velocity and acceleration, respectively, $\dot{\mathbf{r}}^n$ and $\ddot{\mathbf{r}}^n$ are the components of the velocity and acceleration of the rod normal to its centerline, respectively, which can be obtained from the following equations:

$$\dot{\mathbf{r}}^n = \dot{\mathbf{r}} - (\dot{\mathbf{r}} \cdot \mathbf{r}') \cdot \mathbf{r}' \quad (2.23)$$

$$\ddot{\mathbf{r}}^n = \ddot{\mathbf{r}} - (\ddot{\mathbf{r}} \cdot \mathbf{r}') \cdot \mathbf{r}' \quad (2.24)$$

Combining Equations (2.18),(2.19) and (2.20) with (2.14) yields:

$$-(EI\mathbf{r}'')'' + (\lambda\mathbf{r}')' + \mathbf{w} + \mathbf{B} + (P_s A\mathbf{r}')' - C_A\ddot{\mathbf{r}}^n + \tilde{\mathbf{F}}^d = \rho\ddot{\mathbf{r}} \quad (2.25)$$

$$\rho\ddot{\mathbf{r}} + C_A\ddot{\mathbf{r}}^n + (EI\mathbf{r}'')'' - (\lambda\mathbf{r}')' - (P_s A\mathbf{r}')' = \mathbf{w} + \mathbf{B} + \tilde{\mathbf{F}}^d \quad (2.26)$$

$$\rho\ddot{\mathbf{r}} + C_A\ddot{\mathbf{r}}^n + (EI\mathbf{r}''')' - (\tilde{\lambda}\mathbf{r}')' = \tilde{\mathbf{w}} + \tilde{\mathbf{F}}^d \quad (2.27)$$

where

$$\tilde{\mathbf{w}} = \mathbf{w} + \mathbf{B} \quad (2.28)$$

$$\tilde{\lambda} = \lambda + P_s A \quad (2.29)$$

Using $\lambda = T - EI\kappa^2$, we can have

$$\tilde{\lambda} = (T + P_s A) - EI\kappa^2 = \tilde{T} - EI\kappa^2 \quad (2.30)$$

where \tilde{T} is the effective tension in the rod, and $\tilde{\mathbf{w}}$ is the effective weight, or the wet weight. Note that if the effective weight is used, the tension in the equation is effective tension, instead of the actual tension. Equation (2.27) along with the line stretch condition Equation (2.15) or (2.17) are the governing equations for the statics and dynamics of the mooring lines in water.

2.2 Finite Element Modeling

The governing Equations (2.17) and (2.27) can be written in subscript notation:

$$-\rho\ddot{r}_i - C_A\ddot{r}_i^n - (EI r_i''')' + (\tilde{\lambda} r_i')' + \tilde{w}_i + \tilde{F}_i^d = 0 \quad (2.31)$$

$$\frac{1}{2}(r_n' r_n' - 1) - \frac{\lambda}{AE} = \frac{1}{2}(r_n' r_n' - 1) - \frac{\tilde{\lambda} - P_s A}{AE} = 0 \quad (2.32)$$

where the subscripts range from 1 to 3 for the three dimensional problem. Einstein summation notation is employed. Equations (2.17) and (2.27) can be solved by the finite element method. For an element with length L , the variables, $\tilde{\lambda}(s, t)$ and $r_i(s, t)$, along the line can be approximated by:

$$r_i(s, t) = A_k(s)U_{ik}(t) \quad i = 1, 2, 3, \quad k = 1, 2, 3, 4 \quad (2.33)$$

$$\tilde{\lambda}(s, t) = P_m(s)\tilde{\lambda}_m(t) \quad m = 1, 2, 3 \quad (2.34)$$

where A_k and P_m are the interpolating functions, U_{ik} and $\tilde{\lambda}_m$ are the coefficients to be solved and $0 \leq s \leq L$.

Applying Galerkin's method to the Equation (2.31) over the length of the element yields:

$$\int_0^L \delta r_i [-\rho \ddot{r}_i - C_A \ddot{r}_i^n - (E I r_i'')'' + (\tilde{\lambda} r_i')' + \tilde{w}_i + \tilde{F}_i^d] ds = 0 \quad (2.35)$$

Since δr_i and $\delta U_{ii}(t)$ are arbitrary, we can obtain

$$\delta U_{ii}(t) \int_0^L A_l [-\rho \ddot{r}_i - C_A \ddot{r}_i^n - (E I r_i'')'' + (\tilde{\lambda} r_i')' + \tilde{w}_i + \tilde{F}_i^d] ds = 0 \quad (2.36)$$

$$\int_0^L A_l [-\rho \ddot{r}_i - C_A \ddot{r}_i^n - (E I r_i'')'' + (\tilde{\lambda} r_i')' + \tilde{w}_i + \tilde{F}_i^d] ds = 0 \quad (2.37)$$

Integrating the terms in Equation (2.37) by parts results in

$$\int_0^L [A_l (\rho \ddot{r}_i + C_A \ddot{r}_i^n) + E I A_l'' r_i'' + A_l' \tilde{\lambda} r_i' - A_l (\tilde{w}_i + \tilde{F}_i^d)] ds = E I r_i'' A_l' |_0^L + [\tilde{\lambda} r_i' - (E I r_i'')'] A_l |_0^L \quad (2.38)$$

The right hand side of the above equation will vanish when the natural boundary condition of the element is applied.

The interpolating function, A_k and P_m , and coefficients, U_{ij} and $\tilde{\lambda}_m$, are defined as follows:

$$A_1 = 1 - 3\xi^2 + 2\xi^3 \quad (2.39)$$

$$A_2 = \xi - 2\xi^2 + \xi^3 \quad (2.40)$$

$$A_3 = 3\xi^2 - 2\xi^3 \quad (2.41)$$

$$A_4 = -\xi^2 + \xi^3 \quad (2.42)$$

$$P_1 = 1 - 3\xi + 2\xi^2 \quad (2.43)$$

$$P_2 = 4\xi(1 - \xi) \quad (2.44)$$

$$P_3 = \xi(2\xi - 1) \quad (2.45)$$

$$U_{i1} = r_i(0, t) \quad U_{i2} = Lr'_i(0, t) \quad (2.46)$$

$$U_{i3} = r_i(L, t) \quad U_{i4} = Lr'_i(L, t) \quad (2.47)$$

$$\tilde{\lambda}_1 = \tilde{\lambda}(0, t) \quad \tilde{\lambda}_2 = \tilde{\lambda}\left(\frac{L}{2}, t\right) \quad \tilde{\lambda}_3 = \tilde{\lambda}(L, t) \quad (2.48)$$

where $\xi = s/L$.

Applying Galerkin's method to the stretch condition (2.17) yields:

$$\int_0^L P_m \left[\frac{1}{2} (r'_n r'_n - 1) - \frac{\tilde{\lambda} - P_s A}{AE} \right] ds = 0 \quad (2.49)$$

where m and $r = 1, 2, 3$.

Substituting Equations (2.33) and (2.34) into Equation (2.38) and integrating the equation term by term results in the discretized form of equation of motion as follows:

$$(M_{ijkl} + M_{ijkl}^a) \ddot{U}_{jk} + (K_{ijkl}^1 + \tilde{\lambda}_n K_{nijlk}^2) U_{jk} - F_{il} = 0 \quad (2.50)$$

where

$$M_{ijkl} = \int_0^L \rho A_l A_k \delta_{ij} ds \quad (2.51)$$

$$M_{ijkl}^a = C_A \left[\int_0^L A_l A_k \delta_{ij} ds - \left(\int_0^L A_l A_k A'_s A'_t ds \right) U_{it} U_{js} \right] \quad (2.52)$$

$$K_{ijkl}^1 = \int_0^L E I A'_l A'_k \delta_{ij} ds \quad (2.53)$$

$$K_{nijlk}^2 = \int_0^L P_n A'_l A'_k \delta_{ij} ds \quad (2.54)$$

$$F_{il} = \int_0^L (\tilde{w}_i + \tilde{F}_i^d) A_l ds \quad (2.55)$$

where δ_{ij} is the Kronecker Delta function.

Similarly, substituting Equations (2.33) and (2.34) into Equation (2.49) and integrating term by term, we can have

$$G_m = A_{mil} U_{kl} U_{ki} - B_m - C_{mt} \tilde{\lambda}_t + C_{mt} A P_{St} = 0 \quad (2.56)$$

$$A_{mil} = \frac{1}{2} \int_0^L P_m A'_i A'_l ds \quad (2.57)$$

$$B_m = \frac{1}{2} \int_0^L P_m ds \quad (2.58)$$

$$C_{mt} = \frac{1}{AE} \int_0^L P_m P_t ds \quad (2.59)$$

where $m = 1, 2, 3$, $i, l = 1, 2, 3, 4$.

In Equation (2.56), P_s is approximated by

$$P_s = P_m P_{Sm} \quad (2.60)$$

where

$$P_{S1} = P_s(0, t) \quad P_{S2} = P_s\left(\frac{L}{2}, t\right) \quad P_{S3} = P_s(L, t) \quad (2.61)$$

The hydrostatic pressure can be expressed as

$$P_s = \rho g h = -\rho g r_3 \quad (2.62)$$

Combining Equations (2.33) and (2.62) yields:

$$P_{S1} = -\rho g U_{31} \quad (2.63)$$

$$P_{S2} = -\rho g (0.5U_{31} + 0.125U_{32} + 0.5U_{33} - 0.125U_{34}) \quad (2.64)$$

$$P_{S3} = -\rho g U_{33} \quad (2.65)$$

We can see from Equations (2.50) and (2.56) that there are 12 second-order ordinary differential equations and 3 algebraic equations. Note that all these equations are nonlinear.

2.3 Formulation for Static Problem

For the static problem, the inertia term in Equation (2.50) is neglected. The governing differential equations of rod are reduced to

$$R_{il} = (K_{ijlk}^1 + \tilde{\lambda}_n K_{nijlk}^2) U_{jk} - F_{il} = 0 \quad (2.66)$$

$$G_m = A_{mil} U_{kl} U_{ki} - B_m - C_{mt} \tilde{\lambda}_t + C_{mt} A P_{St} = 0 \quad (2.67)$$

where F_{il} is the static force term including the gravity force, the drag force due to the steady current and other applied static forces on the line.

Newton's method is used to solve the nonlinear equations iteratively. Using Taylor series expansion to the two equations above about the estimated solution or the solution from previous n th iteration, $U^{(n)}$ and $\tilde{\lambda}^{(n)}$, and neglecting the higher order terms, we obtain:

$$R_{il}^{(n+1)} = R_{il}^{(n)} + \frac{\partial R_{il}}{\partial U_{jk}} (\Delta U_{jk}) + \frac{\partial R_{il}}{\partial \tilde{\lambda}_n} (\Delta \tilde{\lambda}_n) = 0 \quad (2.68)$$

$$G_m^{(n+1)} = G_m^{(n)} + \frac{\partial G_m}{\partial U_{jk}} (\Delta U_{jk}) + \frac{\partial G_m}{\partial \tilde{\lambda}_n} (\Delta \tilde{\lambda}_n) = 0 \quad (2.69)$$

We can rewrite the equation in a matrix form as

$$\begin{pmatrix} K_{ijlk}^{t0(n)} & K_{iln}^{t1(n)} \\ D_{mjk}^{t0(n)} + D_{mt}^{t0(n)} & D_{mn}^{t1(n)} \end{pmatrix} \begin{Bmatrix} \Delta U_{jk} \\ \Delta \tilde{\lambda}_n \end{Bmatrix} = \begin{Bmatrix} -R_{il}^{(n)} \\ -G_m^{(n)} \end{Bmatrix} \quad (2.70)$$

where

$$\frac{\partial R_{il}}{\partial U_{jk}} = K_{ijkl}^{t0(n)} = K_{ijkl}^1 + \tilde{\lambda}_n^{(n)} K_{nijlk}^2 \quad (2.71)$$

$$\frac{\partial R_{il}}{\partial \tilde{\lambda}_n} = K_{iln}^{t1(n)} = K_{nijlk}^2 U_{jk}^{(n)} \quad (2.72)$$

$$D_{mjk}^{t0(n)} = \frac{\partial}{\partial U_{jk}} \int_0^L P_m \left[\frac{1}{2} (A'_p U_{rp})(A'_q U_{rq}) \right] ds \quad (2.73)$$

$$= \int_0^L P_m \left(\frac{1}{2} A'_k A'_q U_{jq} + \frac{1}{2} A'_k A'_p U_{jp} \right) ds \quad (2.74)$$

$$= \int_0^L P_m A'_k A'_q ds U_{jq}^{(n)} \quad (2.75)$$

$$D_{mt}^{t0(n)} = \frac{\partial}{\partial U_{jk}} (C_{mt} A P_{St}^{(n)}) \quad (2.76)$$

$$\frac{\partial G_m}{\partial \tilde{\lambda}_n} = D_{mn}^{t1(n)} = \int_0^L \left(-\frac{1}{AE} P_m P_n \right) ds \quad (2.77)$$

$$R_{il}^{(n)} = (K_{ijkl}^1 + \tilde{\lambda}_n K_{ijlk}^2) U_{jk}^{(n)} - F_{il} \quad (2.78)$$

$$G_m^{(n)} = A_{mil} U_{kl}^{(n)} U_{ki}^{(n)} - B_m - C_{mt} \tilde{\lambda}_t^{(n)} + C_{mt} A P_{St}^{(n)} \quad (2.79)$$

$$i, j, m, n, r, t = 1, 2, 3, \quad l, k, p, q = 1, 2, 3, 4$$

At each iteration, there are 15 linear algebraic equations for each element. The subscript arrangement in the above equations is not convenient for the numerical solution, thus a renumbering system is employed as follows:

$$\text{DOF of } U_{il} = \begin{bmatrix} 1 & 2 & 9 & 10 \\ 3 & 4 & 11 & 12 \\ 5 & 6 & 13 & 14 \end{bmatrix} \quad \text{for } i = 1, 2, 3 \quad l = 1, 2, 3, 4 \quad (2.80)$$

$$\text{DOF of } \tilde{\lambda}_m = \begin{bmatrix} 7 & 8 & 15 \end{bmatrix} \quad \text{for } m = 1, 2, 3 \quad (2.81)$$

After renumbering, Equation (2.70) can be rewritten in the following form:

$$[K^{(n)}]\{\Delta y\} = \{F^{(n)}\} \quad (2.82)$$

where $[K^{(n)}]$ is the stiffness matrix and the vector $\{\Delta y\}$ consists of the variables ΔU_{jk} and $\Delta \tilde{\lambda}_m$.

$$\{\Delta y\} = \begin{bmatrix} \Delta U_{11}, & \Delta U_{12}, & \Delta U_{21}, & \Delta U_{22}, & \Delta U_{31}, & \Delta U_{32}, & \Delta \tilde{\lambda}_1, & \Delta \tilde{\lambda}_2, & \Delta U_{13}, & \Delta U_{14}, \\ \Delta U_{23}, & \Delta U_{24}, & \Delta U_{33}, & \Delta U_{34}, & \Delta \tilde{\lambda}_3 \end{bmatrix}^T \quad (2.83)$$

$\{F^{(n)}\}$ is the force vector:

$$\{F^{(n)}\} = \begin{bmatrix} -R_{11}, & -R_{12}, & -R_{21}, & -R_{22}, & -R_{31}, & -R_{32}, & -G_1, & -G_2, & -R_{13}, & -R_{14}, \\ -R_{23}, & -R_{24}, & -R_{33}, & -R_{34}, & -G_3 \end{bmatrix}^T \quad (2.84)$$

After the element equations are assembled and the boundary conditions are applied, the assembled equations can be solved by Gauss elimination. An iterative procedure is applied with initially guessed values of U and $\tilde{\lambda}$. The variables are updated by $y^{(n+1)} = y^{(n)} + \Delta y$ after solving the assembled equations. The generalized stiffness matrix, K , and force vector, F , in the equation are recalculated to solve Δy again. This procedure continues until Δy is smaller than a prescribed tolerance. The equilibrium position and the tension of the mooring line can be obtained.

2.4 Formulation for Dynamic Problem - Time Domain Integration

According to the work of Ran (2000), the equation of motion (2.50) can be rewritten as:

$$\begin{aligned} (\hat{M}_{ijkl})\ddot{U}_{jk} &= -(K_{ijkl}^1 + \tilde{\lambda}_n K_{nijlk}^2)U_{jk} + F_{il} \\ &= -F_{il}^1 - F_{il}^2 + F_{il} = \hat{F}_{il} \end{aligned} \quad (2.85)$$

where

$$\hat{M}_{ijkl} = M_{ijkl} + M_{ijkl}^a \quad (2.86)$$

$$F_{il}^1 = K_{ijkl}^1 U_{jk} \quad (2.87)$$

$$F_{il}^2 = \tilde{\lambda}_n K_{nijlk}^2 U_{jk} \quad (2.88)$$

The dynamic solution can be obtained by solving equation (2.85) and (2.56).

Equation (2.85) is a second-order differential equation and equation (2.56) is an algebraic equation without time derivatives. In order to derive the integration scheme, we use a first order differential equation system to replace Equation (2.85):

$$\hat{M}_{ijkl}\dot{V}_{jk} = \hat{F}_{il} \quad (2.89)$$

$$\dot{U}_{jk} = V_{jk} \quad (2.90)$$

Integrating the above two equations from time $t^{(n)}$ at time step n to $t^{(n+1)}$ at time step $n + 1$ yields

$$\int_{t^{(n)}}^{t^{(n+1)}} \hat{M}_{ijkl}\dot{V}_{jk}dt = \int_{t^{(n)}}^{t^{(n+1)}} \hat{F}_{il}dt \quad (2.91)$$

$$\int_{t^{(n)}}^{t^{(n+1)}} \dot{U}_{jk} dt = \int_{t^{(n)}}^{t^{(n+1)}} V_{jk} dt \quad (2.92)$$

where \hat{M}_{ijkl} is not constant since it contains the added mass term M_{ijkl}^a which is a function of the line geometry, thus it varies with time. Assuming \hat{M}_{ijkl} in the time interval, $\Delta t = t^{(n+1)} - t^{(n)}$, is constant, we can simplify the integration of the left hand side of Equation (2.91) as follows:

$$\hat{M}_{ijkl}^{(n+\frac{1}{2})} V_{jk}^{(n+1)} - \hat{M}_{ijkl}^{(n+\frac{1}{2})} V_{jk}^{(n)} = \int_{t^{(n)}}^{t^{(n+1)}} \hat{F}_{il} dt \quad (2.93)$$

where $\hat{M}_{ijkl}^{(n+\frac{1}{2})}$ is the mass at time $t^{(n)} + \frac{\Delta t}{2}$. Based upon the second-order Adams-Moulton integration, Equation (2.92) can be written as:

$$U_{jk}^{(n+1)} - U_{jk}^{(n)} = \frac{\Delta t}{2} [V_{jk}^{(n+1)} + V_{jk}^{(n)}] \quad (2.94)$$

Re-arranging the above two equations, we obtain:

$$V_{jk}^{(n+1)} = \frac{2}{\Delta t} \Delta U_{jk} - V_{jk}^{(n)} \quad (2.95)$$

$$\frac{4}{\Delta t^2} \hat{M}_{ijkl}^{(n+\frac{1}{2})} \Delta U_{jk} = \frac{4}{\Delta t} \hat{M}_{ijkl}^{(n+\frac{1}{2})} V_{jk}^{(n)} + \frac{2}{\Delta t} \int_{t^{(n)}}^{t^{(n+1)}} \hat{F}_{il} dt \quad (2.96)$$

where

$$\Delta U_{jk} = U_{jk}^{(n+1)} - U_{jk}^{(n)} \quad (2.97)$$

$$\int_{t^{(n)}}^{t^{(n+1)}} \hat{F}_{il} dt = - \int_{t^{(n)}}^{t^{(n+1)}} F_{il}^1 dt - \int_{t^{(n)}}^{t^{(n+1)}} F_{il}^2 dt + \int_{t^{(n)}}^{t^{(n+1)}} F_{il} dt \quad (2.98)$$

Applying the Adams-Moulton method to the first and the second terms at the right hand side of the above equation, we can obtain:

$$\int_{t^{(n)}}^{t^{(n+1)}} F_{il}^1 dt = \frac{\Delta t}{2} (F_{il}^{1(n+1)} + F_{il}^{1(n)}) = \frac{\Delta t}{2} [K_{ijlk}^1 \Delta U_{jk} + 2K_{ijlk}^1 U_{jk}^{(n)}] \quad (2.99)$$

$$\begin{aligned} \int_{t^{(n)}}^{t^{(n+1)}} F_{il}^2 dt &= \frac{\Delta t}{2} (F_{il}^{2(n+1)} + F_{il}^{2(n)}) \quad (2.100) \\ &= \frac{\Delta t}{2} (\tilde{\lambda}_n^{(n+1)} K_{nijlk}^2 U_{jk}^{(n+1)} + \tilde{\lambda}_n^{(n)} K_{nijlk}^2 U_{jk}^{(n)}) \\ &\approx \frac{\Delta t}{2} (\tilde{\lambda}_n^{(n+\frac{1}{2})} K_{nijlk}^2 U_{jk}^{(n+1)} + \tilde{\lambda}_n^{(n+\frac{1}{2})} K_{nijlk}^2 U_{jk}^{(n)}) \\ &= \frac{\Delta t}{2} [(\tilde{\lambda}_n^{(n-\frac{1}{2})} + \Delta \tilde{\lambda}) K_{nijlk}^2 (U_{jk}^{(n)} + \Delta U_{jk}) + (\tilde{\lambda}_n^{(n-\frac{1}{2})} + \Delta \tilde{\lambda}) K_{nijlk}^2 U_{jk}^{(n)}] \\ &\approx \frac{\Delta t}{2} [2\tilde{\lambda}_n^{(n-\frac{1}{2})} K_{nijlk}^2 U_{jk}^{(n)} + 2K_{nijlk}^2 U_{jk}^{(n)} \Delta \tilde{\lambda}_n + \tilde{\lambda}_n^{(n-\frac{1}{2})} K_{nijlk}^2 \Delta U_{jk}] \end{aligned}$$

where $\Delta \tilde{\lambda}_n = \tilde{\lambda}_n^{(n+\frac{1}{2})} - \tilde{\lambda}_n^{(n-\frac{1}{2})}$. The third term in Equation (2.98) is the applied force F_{il} , including gravity force and hydrodynamic forces, and etc. Note that the hydrodynamic forces calculated by Morrison's equation are unknown at time step $n+1$ since the hydrodynamic forces are functions of the unknown rod position and velocity. Therefore the Adams-Bashforth explicit scheme can be used for the integral:

$$\int_{t^{(n)}}^{t^{(n+1)}} F_{il} dt = \frac{\Delta t}{2} (3F_{il}^{(n)} - F_{il}^{(n-1)}) \quad (2.101)$$

For the first time step, $\int_{t^{(n)}}^{t^{(n+1)}} F_{il} dt = \Delta t F_{il}^{(0)}$

Combining equations (2.93), (2.94), (2.99), (2.100) and (2.101), we can obtain the integration scheme for the equation of motion (2.85):

$$\left[\frac{4}{\Delta t^2} \hat{M}_{ijlk}^{(n+\frac{1}{2})} + K_{ijlk}^1 + \tilde{\lambda}_n^{(n-\frac{1}{2})} K_{nijlk}^2 \right] \Delta U_{jk} + 2K_{nijlk}^2 U_{jk}^{(n)} \Delta \tilde{\lambda}_n = \quad (2.102)$$

$$\frac{4}{\Delta t} \hat{M}_{ijkl}^{(n+\frac{1}{2})} V_{jk}^{(n)} + (3F_{il}^{(n)} - F_{il}^{(n-1)}) - 2K_{ijkl}^1 U_{jk}^{(n)} - 2\tilde{\lambda}_n^{(n-\frac{1}{2})} K_{nijlk}^2 U_{jk}^{(n)} \quad (2.103)$$

The mass term can be approximated by using the Adams-Bashforth method

$$\hat{M}_{ijkl}^{(n+\frac{1}{2})} = \frac{1}{2}(3\hat{M}_{ijkl}^{(n)} - \hat{M}_{ijkl}^{(n-1)}) \quad (2.104)$$

and $\tilde{\lambda}^{(n-\frac{1}{2})}$ can be approximated by using the trapezoidal rule:

$$\tilde{\lambda}^{(n-\frac{1}{2})} = \frac{1}{2}(\tilde{\lambda}^{(n)} + \tilde{\lambda}^{(n-1)}) \quad (2.105)$$

For the stretch condition, Equation (2.56), we can approximate $G_m^{(n+1)}$ at time step $n+1$ from $G_m^{(n)}$ using Taylor expansion, i.e.,

$$0 = 2G_m^{(n+1)} \approx 2G_m^{(n)} + 2\frac{\partial G_m^{(n)}}{\partial U_{jk}} \Delta U_{jk} + 2\frac{\partial G_m^{(n)}}{\partial \tilde{\lambda}_n} \Delta \tilde{\lambda}_n = 2G_m^{(n)} + 2K_{mijkl}^2 U_{il} \Delta U_{jk} + 2D_{mn}^{t1(n)} \Delta \tilde{\lambda}_n \quad (2.106)$$

Equations (2.102) and (2.106) can be rewritten in a form similar to the static problem:

$$\hat{K}_{ijkl}^{t0(n)} \Delta U_{jk} + \hat{K}_{iln}^{t1(n)} \Delta \tilde{\lambda}_n = \hat{R}_{il}^{(n)} \quad (2.107)$$

$$\hat{D}_{mjk}^{t0(n)} \Delta U_{jk} + \hat{D}_{mn}^{t1(n)} \Delta \tilde{\lambda}_n = \hat{G}_m^{(n)} \quad (2.108)$$

where

$$\hat{K}_{ijkl}^{t0(n)} = \frac{2}{\Delta t^2} (3\hat{M}_{ijkl}^{(n)} - \hat{M}_{ijkl}^{(n-1)}) + K_{ijkl}^1 + \tilde{\lambda}_n^{(n-\frac{1}{2})} K_{nijlk}^2 \quad (2.109)$$

$$\hat{K}_{iln}^{t1(n)} = 2K_{nijlk}^2 U_{jk}^{(n)} \quad (2.110)$$

$$\hat{D}_{mjk}^{t0(n)} = 2K_{mijkl}^2 U_{il} \quad (2.111)$$

$$\hat{D}_{mn}^{t1(n)} = 2D_{mn}^{t1(n)} \quad (2.112)$$

$$\hat{R}_{il}^{(n)} = \frac{2}{\Delta t} (3\hat{M}_{ijkl}^{(n)} - \hat{M}_{ijkl}^{(n-1)}) V_{jk}^{(n)} + (3F_{il}^{(n)} - F_{il}^{(n-1)}) - 2K_{ijkl}^1 U_{jk}^{(n)} - 2\tilde{\lambda}_n^{(n-\frac{1}{2})} K_{nijlk}^2 U_{jk}^{(n)} \quad (2.113)$$

$$\hat{G}_m^{(n)} = -2G_m^{(n)} \quad (2.114)$$

where the superscript n indicating the n th time step.

The subscript arrangement in the above equations is not convenient for numerical solution, thus a renumbering system is employed as follows

$$\{\Delta y\} = [\Delta U_{11}, \Delta U_{12}, \Delta U_{21}, \Delta U_{22}, \Delta U_{31}, \Delta U_{32}, \Delta \tilde{\lambda}_1, \Delta \tilde{\lambda}_2, \Delta U_{13}, \Delta U_{14}, \Delta U_{23}, \Delta U_{24}, \Delta U_{33}, \Delta U_{34}, \Delta \tilde{\lambda}_3]^T \quad (2.115)$$

Similar to the static problem, the final equation for a rod element can be written as

$$[K^{(n)}]\{\Delta y\} = \{F^{(n)}\} \quad (2.116)$$

where $\{F^{(n)}\}$ is the force vector:

$$\{F^{(n)}\} = [-R_{11}, -R_{12}, -R_{21}, -R_{22}, -R_{31}, -R_{32}, -G_1, -G_2, -R_{13}, -R_{14}, -R_{23}, -R_{24}, -R_{33}, -R_{34}, -G_3]^T \quad (2.117)$$

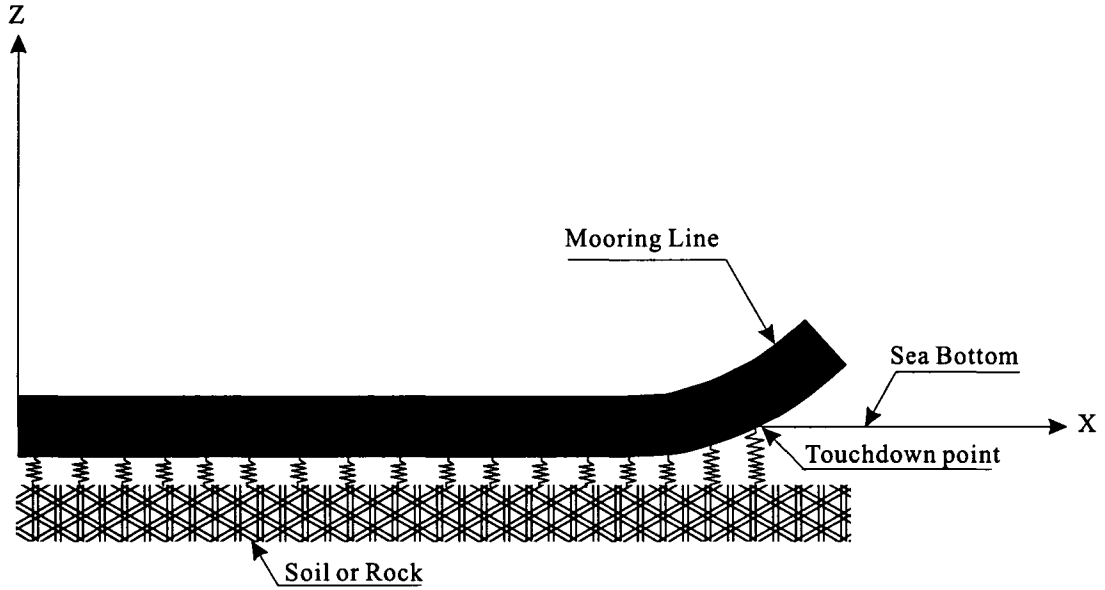


Figure 2-2: Sea Bottom Boundary Condition

2.5 The Sea Bottom Boundary Condition

The mooring lines cannot penetrate the sea bottom. Assuming the sea bottom is flat and elastic, the sea bottom can be modeled by an elastic layer (spring mat).

The distributed bottom support force in vertical direction can be expressed in the following form (Chen, 2002):

$$q^{spring} = \begin{cases} \frac{w}{R}\{R - (r_3 - Z_{bottom})\} & R - (r_3 - Z_{bottom}) > 0 \\ 0 & R - (r_3 - Z_{bottom}) \leq 0 \end{cases} \quad (2.118)$$

In order to consider the bottom support force, an extra term representing the distributed spring force is added to the equation of motion of the mooring line. Multiplying both sides of the above equation by the shape function A_l and integrating it with respect to s along the length of an element, which touches the bottom, we can obtain

$$\int_0^L q^{spring} A_l(s) ds = \mu_{lm} \left\{ \frac{w}{R} (R + Z_{bottom}) \right\} |_m - \gamma_{lkm} U_{3k} \left\{ \frac{w}{R} \right\} |_m \quad (2.119)$$

where

$$\mu_{lm} = L \int_{\xi_1}^{\xi_2} A_l P_m ds \quad (2.120)$$

$$\gamma_{lkm} = L \int_{\xi_1}^{\xi_2} A_l A_k P_m ds \quad (2.121)$$

In the dynamic analysis of mooring lines, the bottom friction force is considered as follows:

$$q^{friction} = \begin{cases} C_f \mu_f \frac{r'}{|r'|} & R - (r_3 - Z_{bottom}) > 0 \\ 0 & R - (r_3 - Z_{bottom}) \leq 0 \end{cases} \quad (2.122)$$

$$C_f = \begin{cases} -1 & V_t > C_V \\ -\frac{V_t}{C_V} & V_t \leq C_V \\ 1 & V_t < -C_V \end{cases} \quad (2.123)$$

$$\int_0^L q^{friction} A_l(s) ds = \mu_{lm} C_f \mu_f \left\{ w \frac{r'}{|r'|} \right\} |_m \quad (2.124)$$

where V_t is the tangential velocity of the mooring line, C_V is the tolerance of tangential velocity, and μ_f is the dynamic bottom friction coefficient.

Due to the effect of the ocean bottom, the coefficients, μ_{lm} and γ_{lkm} , are not constant for the element around the touchdown point. They are integrated separately over the portion of the element that contacts the sea floor.

Chapter 3

Numerical Results

Based on the mathematical formulations in Chapter 2, a computer program, MAPS-Mooring, for static and dynamic mooring analysis, has been developed. Studies have been carried out to verify and validate the developed program.

To validate the static analysis of MAPS-Mooring, the program has been applied to single and multiple mooring lines. A static analysis was first conducted for a simple catenary mooring line. The numerical solutions were compared with the analytical solutions. A moored surface buoy under steady current was also used to verify the load on the mooring line under current. The static analyses were then extended to a mooring system with multiple lines.

To validate the dynamic analysis of the computer program, studies have been carried out for the large amplitude motion of a rigid bar pendulum and a mooring system. The global-coordinate-based finite element method was also applied to conduct the vortex induced vibration (VIV) analysis for a rigid riser.

3.1 Simple Catenary Mooring Line

The first example is a simple catenary mooring line (Garrett, 1982) under a horizontal force at its lower end as shown in Figure 3-1.

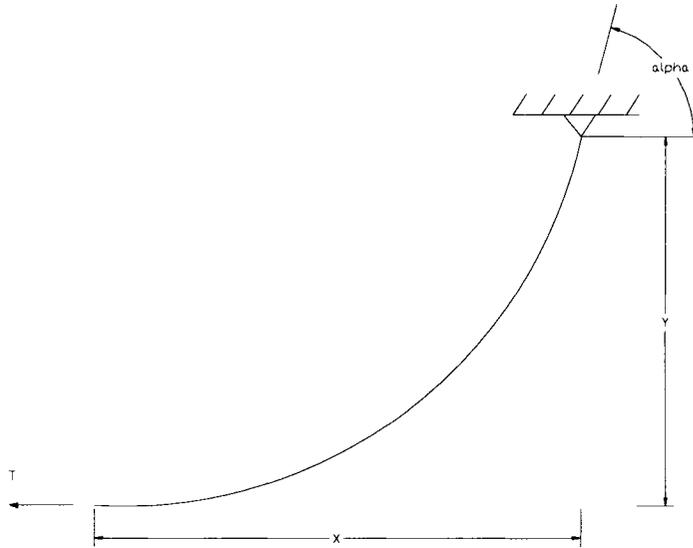


Figure 3-1: Simple Catenary Mooring Line

The configuration of the simple catenary is determined by the dimensionless parameter $\frac{WL}{T}$, where W is the weight per unit length, L is the length of the catenary line and T is the horizontal force. The numerical results obtained using one element and ten equal length elements are compared with the analytical solutions. As shown in Table 3.1, the numerical results agree very well with the analytical solutions. In Table 3.1, α is the angle between the horizontal line and the tangent direction of the mooring line at fairlead as shown in Figure 3-1.

Table 3.1: Catenary - Comparison between Numerical Solutions and Analytical Results

WL/T	α, deg			X/L			Y/L		
	1 element	10 elements	analytical	1 element	10 elements	analytical	1 element	10 elements	analytical
1	45.374	45.000	45.000	0.88138	0.88137	0.88137	0.41426	0.41421	0.41421
2	63.277	63.434	63.435	0.72194	0.72182	0.72182	0.61790	0.61803	0.61803
5	75.705	78.689	78.690	0.46756	0.46249	0.46249	0.82216	0.81981	0.81980
10	80.720	84.289	84.289	0.30168	0.29982	0.29982	0.92065	0.90499	0.90499

3.2 Moored Surface Buoy Under Steady Current

The computer program was applied to determine the static mooring load of a moored surface buoy under steady current (Berteaux, 1976). The surface buoy is moored in 2000 ft of water. The diameter of the mooring line is 0.315 in., and its line density is 0.124 lb/ft. The velocity of uniform current is 4.54 ft/sec. The line angle at the anchor is 30 degrees and the line tension is 3000 lb at the anchor. The normal drag coefficient is 1.8 and the tangential drag to the normal drag ratio is assumed as 0.02.

The computed equilibrium position of mooring line is compared with those by Pote's method (Berteaux, 1976) in Figure 3-3. The agreement is very good.

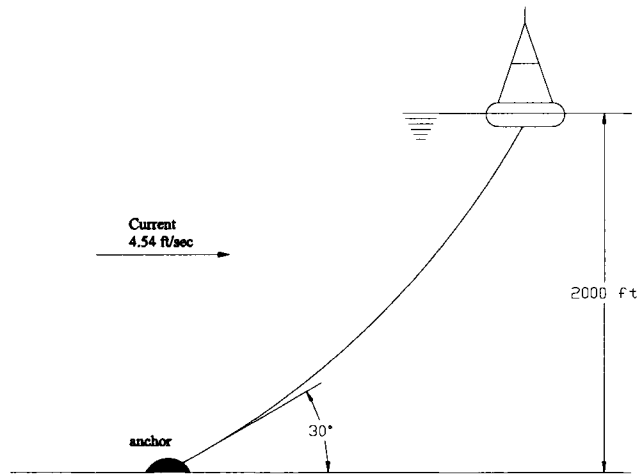


Figure 3-2: Moored Surface Buoy Under Steady Current

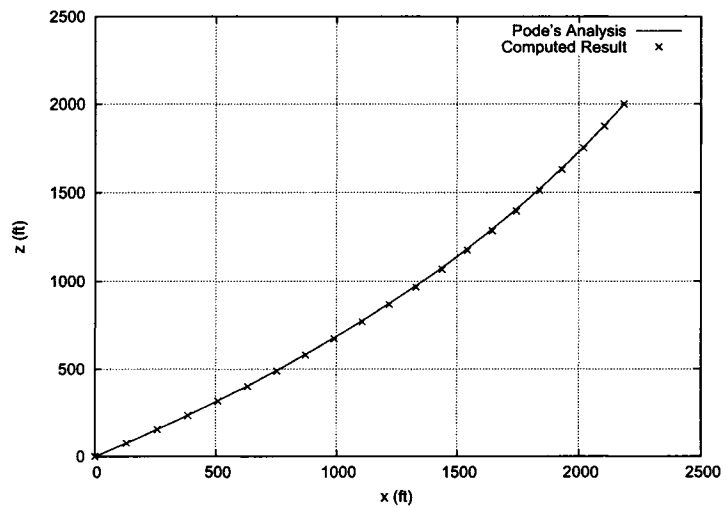


Figure 3-3: Equilibrium Position of Mooring Line under Steady Current

3.3 Multiple Mooring Lines System

The static analyses were then extended to a mooring system with multiple lines. In this case, the mooring system (Brown *et al.*, 1998) consists of eight mooring lines, which have the same properties. Each mooring line has only one segment. Figures 3-4 and 3-5 show the plan view and the three dimensional configuration of the mooring system, respectively. The principal parameters are given as follows:

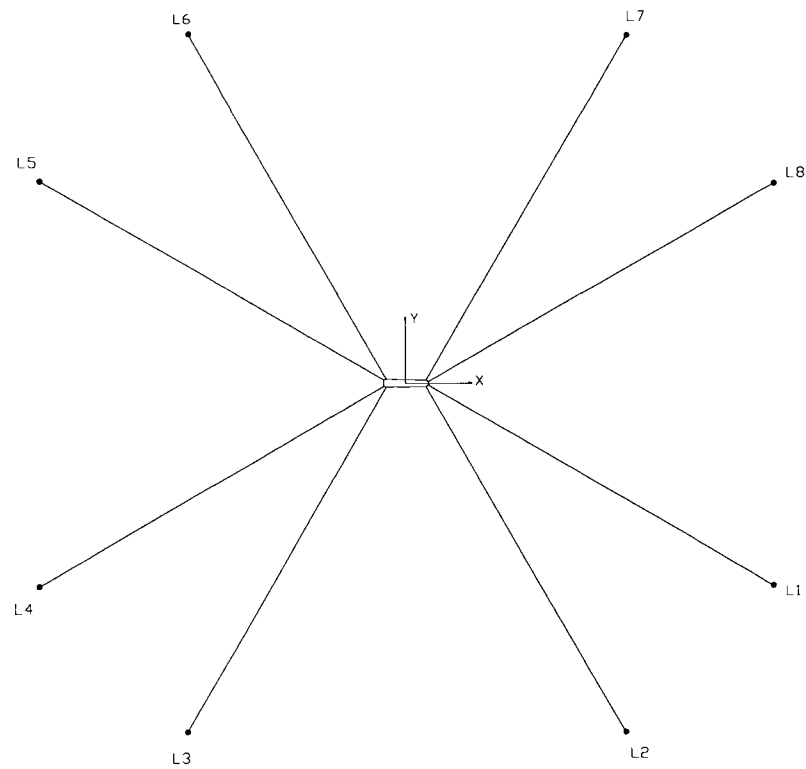


Figure 3-4: Plan View of the Mooring System (Brown and Lyons, 1998)

- Total length for each mooring line: 2485 m
- Weight per unit length: 0.194 kN/m
- Water depth: 180 m

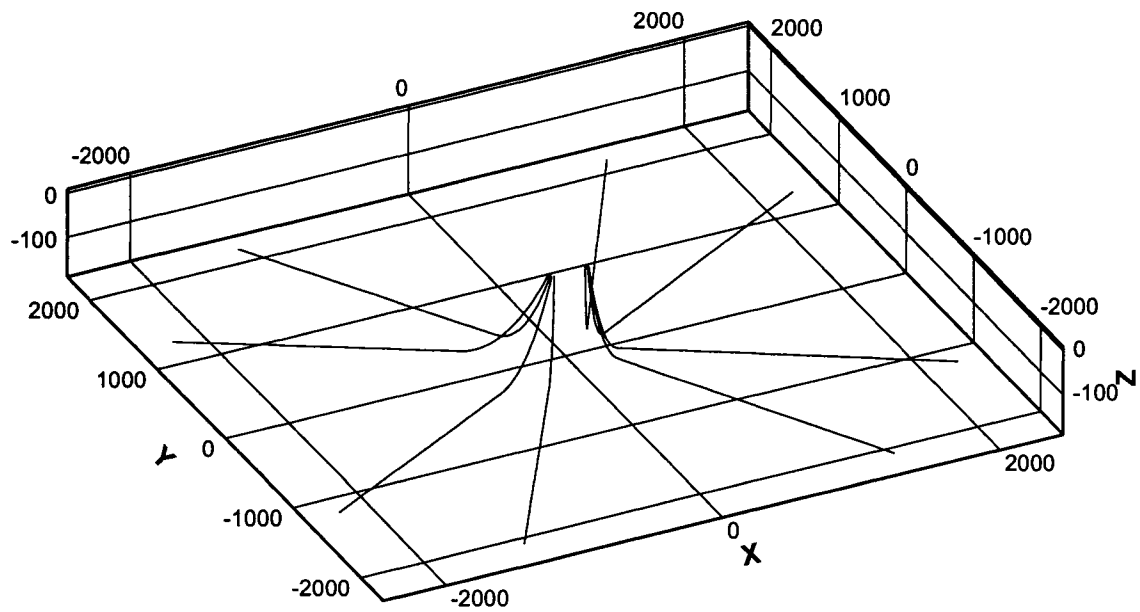


Figure 3-5: Three Dimensional Configuration of the Mooring System

- Pretension: 89.26 kN
- Elasticity: inextensible

The coordinates of fairleads and azimuth angles of the mooring lines are given in Table 3.2. The azimuth angle of each mooring line is measured counter clockwise from X-axis to the mooring line when it is viewed downward along Z-axis.

Since the coordinates of anchor points were not provided in this case, the static analysis for each single mooring line was conducted in order to find the coordinates of the anchor point. This was achieved by the following steps:

- A. The coordinates for the anchor point along the direction of the mooring line was first guessed and the tension of the mooring line was computed by MAPS-Mooring.

Table 3.2: Coordinates of Fairleads and Azimuth Angles of the Mooring Lines

Line No.	X (m)	Y (m)	Z (m)	Azimuth Angle (degree)
1	138.0	-10.0	0.0	30
2	126.0	-20.0	0.0	60
3	-118.0	-23.0	0.0	120
4	-136.0	-20.0	0.0	150
5	-136.0	20.0	0.0	210
6	-118.0	23.0	0.0	240
7	126.0	20.0	0.0	300
8	138.0	10.0	0.0	330

- B. The computed tension was compared with the pretension of the mooring line. If it was greater than the pretension, the anchor point was moved closer to the fairlead point along the direction of the mooring line; otherwise the anchor point was moved farther away from the fairlead point.
- C. This process was repeated until the computed tension was equal to or close enough to the pretension. The coordinate of the anchor point for this mooring line was then determined.

After the location of the anchor point was determined for each mooring line, static analysis of multiple mooring lines was then carried out. By specifying the coordinates of the fairlead points for different offsets of the floating body, the resultant forces and moments were computed for a series of specified coordinates of the fairlead points corresponding to different offsets of the floating body. The computation was carried out for two cases, in which the mooring lines were assumed to be inextensible and extensible, respectively.

The computed surge forces were compared in Figure 3-6 with those by MOOR, a program developed by Brown and Lyons (1998), and those by MOORING-SYSTEM (Lau *et al.*, 2005). Note that the computation by MOOR was based on the inextensible assumption. It can be seen that the results for the inextensible case agree very

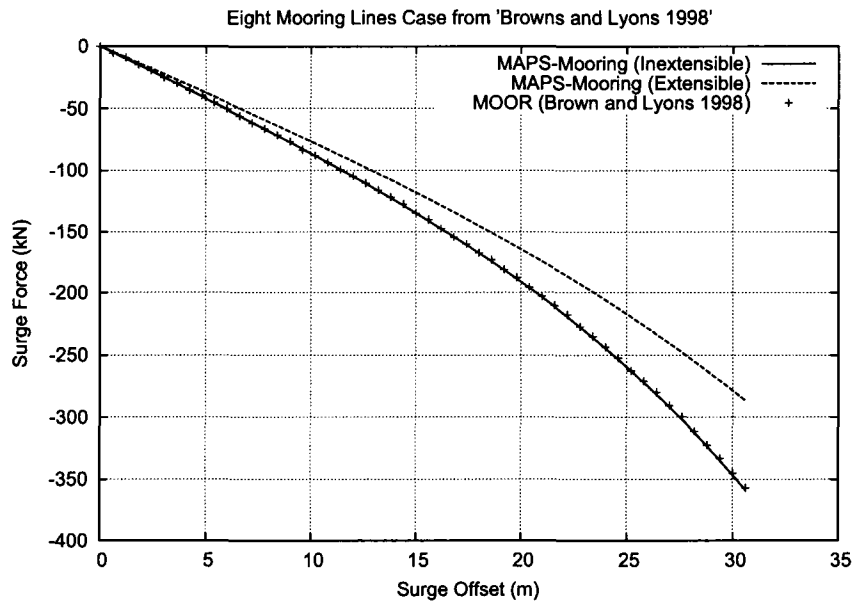


Figure 3-6: Comparison of Results by MAPS-Mooring, MOOR and Mooring-System

well with those by MOOR. It is also shown that the surge forces with the extensible assumption are lower than those with inextensible assumption for the same surge offset. This is due to the fact that the stiffness of the extensible mooring system is less than that of the inextensible mooring system.

3.4 Large-Amplitude Motion of A Rigid Pendulum

The large-amplitude motion of a rigid pendulum has been studied to verify the developed dynamic program.

The uniform rigid bar pendulum, as shown in Figure 3-7, was modeled by a single element with a bending stiffness of 10^{11} lb-ft². The mass per unit length m , the length l and the acceleration of gravity g are 1 slug/ft, 10 ft and 32ft/s², respectively. The bar pendulum is released from rest in a horizontal position. The motion of the bar



Figure 3-7: Initial Position of the Uniform Rigid Bar

pendulum was computed using a time step of 0.01s. The numerical results in Figure 3-8 show that the amplitude of the periodic motion does not change with time and the computed period is equal to the analytical solution, $T = 3.385s$ (Garrett, 1982, Ran, 1997). These demonstrated the great accuracy and stability of the numerical algorithm.

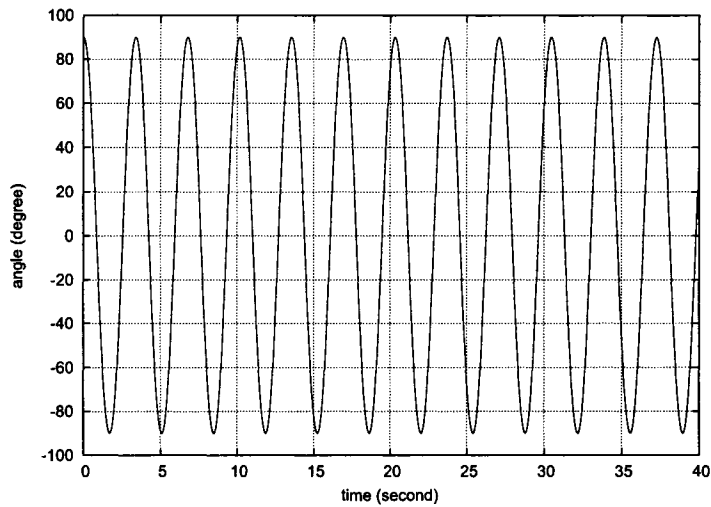


Figure 3-8: Motion of Uniform Rigid Bar

3.5 Validation Studies for Dynamic Analysis

Validation studies were carried out for the dynamics of a mooring system which was tested by Ship Dynamics Laboratory, Canal de Experiencias hidrodinamicas de El Pardo (CEHIPAR) in a scale of 1:16 (Kitney *et al.*, 2001). The characteristics of the mooring line are listed in Table 3.3.

Table 3.3: Characteristics of the Mooring Line Used in the Analysis and Experiments

Mooring Line Data	Prototype	CEHIPAR Model	CEHIPAR Model
	Required	Required	Actual
Water Depth	82.5m	5.0m	5.0m
Scale Factor	1	16.5	
Line Length	711m	43.0m	43.0m
Diameter	140mm	8.5mm	8.0mm
Weight/Length	3202N/m	11.76N/m	11.47N/m
Elastic Modulus	$1.69 \times 10^9 \text{N}$	$3.76 \times 10^5 \text{N}$	$3.83 \times 10^6 \text{N}$

The dynamic analysis was conducted for the prototype model. Firstly, the sensitivity of numerical solutions to the number of elements and the time step was investigated. In the sensitivity study of the number of elements, 20, 40, 80 and 160 elements were used with a fixed time step of 0.05s. In the sensitivity analysis of the time step, 0.2s, 0.1s, 0.05s and 0.025s were used with a fixed number of elements of 80. The numerical results for the sensitivity studies are given in Figures 3-9 and 3-10. As shown in these figures, the dynamic solution converges as the number of elements is increased and the time step is decreased. In the following studies, the number of elements and the time step were chosen as 80 and 0.05s, respectively. Both the numerical solutions and the experimental results were nondimensionalized. The nondimensional line tension, T_{nondim} , is expressed as the ratio of dynamic line tension, $T_{dynamic}$, to the static tension, T_{static} , at the top end of the mooring line. The dynamic

line tension, $T_{dynamic}$, is determined from

$$T_{dynamic} = T_{max} - T_{static}$$

where T_{max} is the maximum line tension.

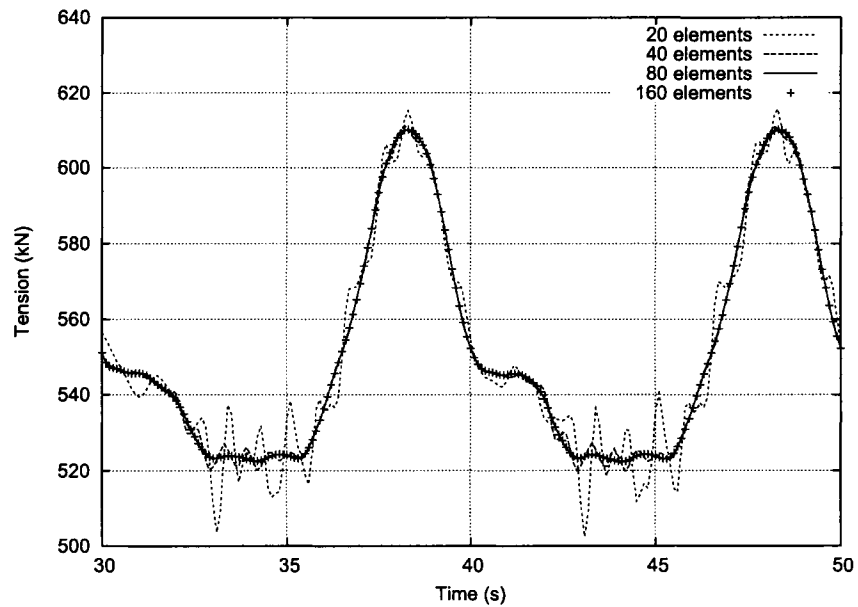


Figure 3-9: Sensitivity to Number of Elements

The dynamic analyses were conducted for various fairlead motions. The amplitude of the fairlead motion, a , was nondimensionalized by the water depth, d . The time series of the top tension for nondimensional amplitudes of 0.03, 0.065, 0.075 and 0.095 are given in Figures 3-11, 3-12, 3-13 and 3-14, respectively. The nondimensional line tensions at various fairlead motions were compared with the experimental data in Figure 3-15. The numerical solutions agree well with the experimental results.

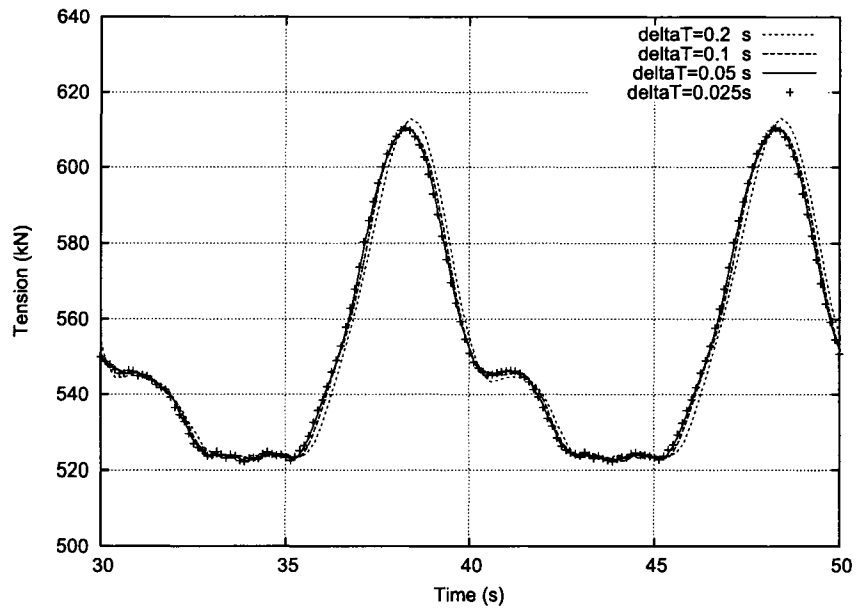


Figure 3-10: Sensitivity to Time Step

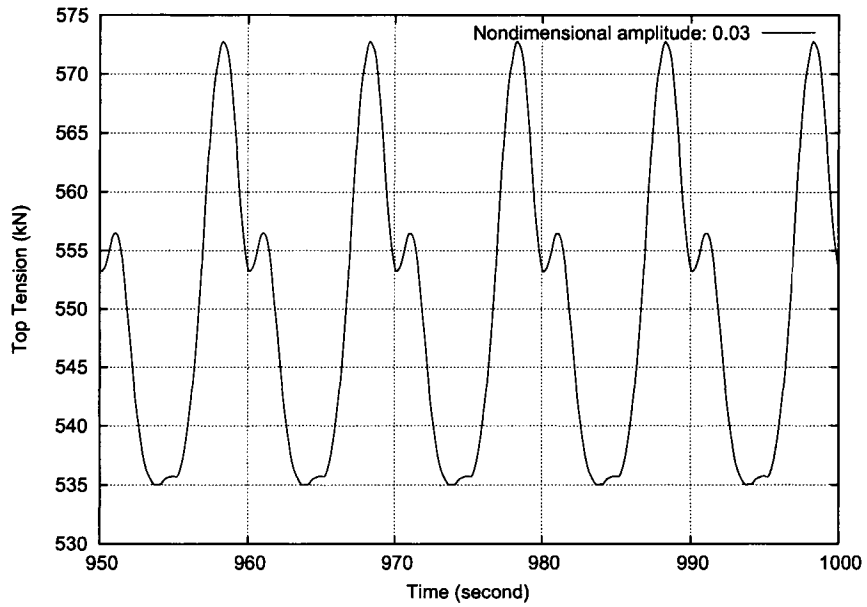


Figure 3-11: Time-domain Tension at Nondimensional Motion Amplitude of 0.03

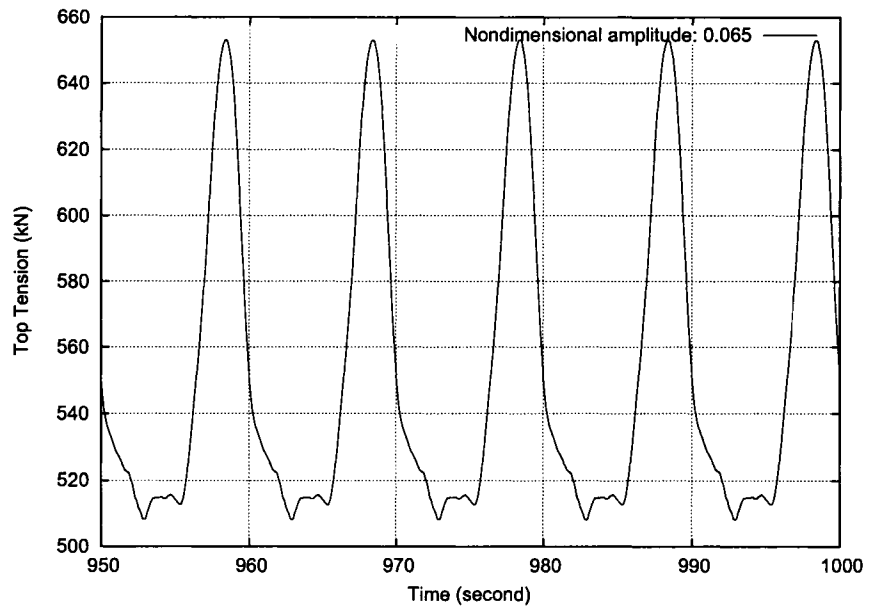


Figure 3-12: Time-domain Tension at Nondimensional Motion Amplitude of 0.065

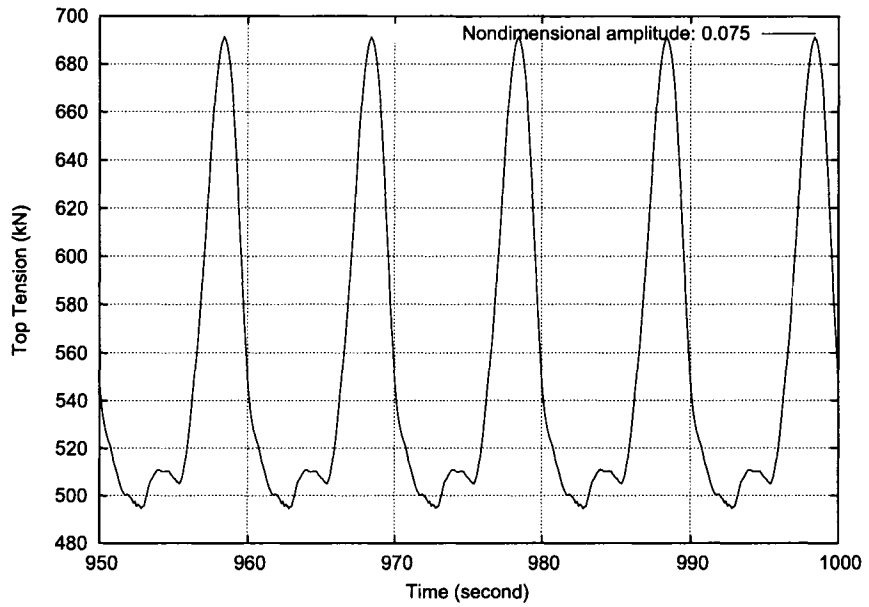


Figure 3-13: Time-domain Tension at Nondimensional Motion Amplitude of 0.075

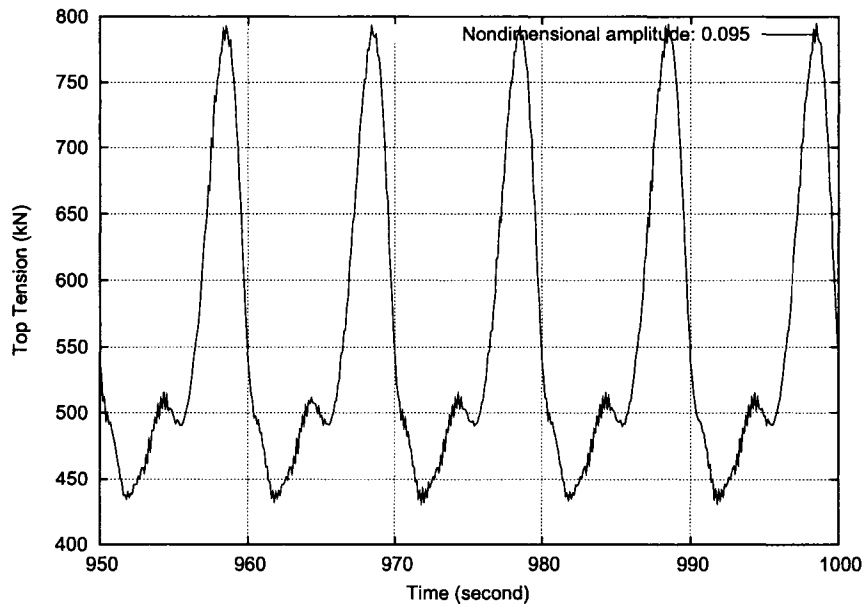


Figure 3-14: Time-domain Tension at Nondimensional Motion Amplitude of 0.095

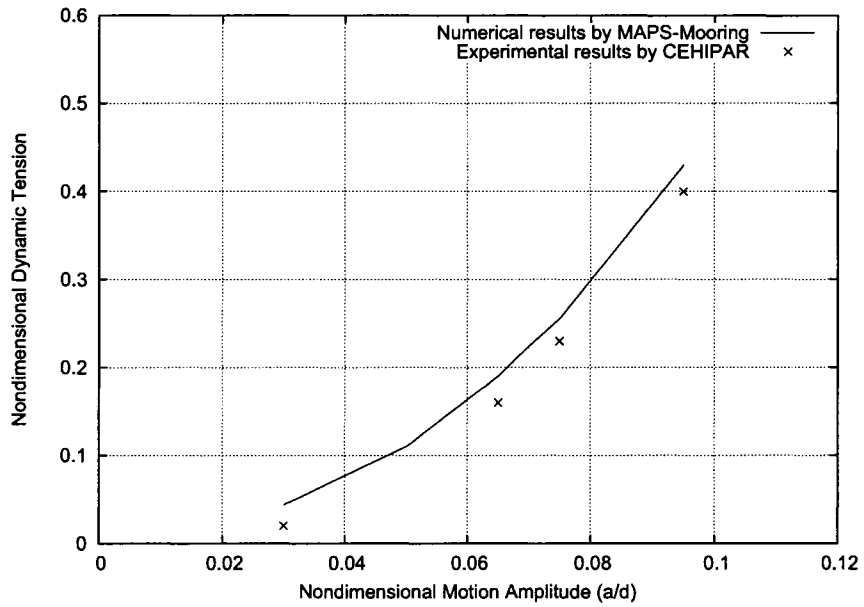


Figure 3-15: Nondimensional Dynamic Line Tension

3.6 Vortex Induced Vibration of Marine Riser

The global-coordinate-based finite element method was also applied to the vortex induced vibration (VIV) analysis of a rigid riser with only single mode. The process for the VIV analysis of risers is the same as that of the analysis of mooring lines, except the computation of the hydrodynamic loads. For a VIV analysis, not only the drag forces but also the lift forces are considered in the analysis. The procedure of the VIV analysis is given below (Spencer, 2006):

1. Assuming the initial value of reduced velocity V_r , drag coefficient C_d , lift coefficient C_l and added mass coefficient C_m , the initial apparent period of cross-flow motion is computed by

$$T_{apparent} = \frac{V_r D}{U} \quad (3.1)$$

where D is the diameter of the riser, U is the velocity of the current.

2. The responses of the riser, including the displacement and the velocity, are computed at each time step. The cycle of the VIV motion is determined from zero up-crossings on the displacement curve of the riser.
3. After each cycle, the apparent period, $T_{apparent}$, and maximum and minimum peak motion amplitude, A^+ and A^- , can be obtained and therefore the reduced velocity, V_r , and the amplitude ratio, A^* , can be computed by

$$V_r = \frac{UT_{apparent}}{D} \quad (3.2)$$

$$A^* = \frac{A^+ - A^-}{2D} \quad (3.3)$$

4. By using the newly obtained reduced velocity, V_r , and amplitude ratio, A^* , the new added mass coefficient C_m is interpolated by $C_m = f(A^*, V_r)$, which are obtained from experiments.

5. The natural frequency F_n of the riser is recomputed according to the new added mass coefficient C_m . The reduced velocity, V_r , is recalculated by $V_r = \frac{U}{F_n D}$.
6. Repeat Steps 5 and 6 until V_r and C_m are compatible, which means that the value of reduce velocity, V_r , obtained at Step 5 is sufficiently close to that obtained at Step 3.
7. The lift coefficient, C_l , and the drag coefficient, C_d , are interpolated from the experimental database, $C_l = g(A^*, V_r)$, by using the final V_r and C_m . The typical plot of C_l is shown in 3-16.

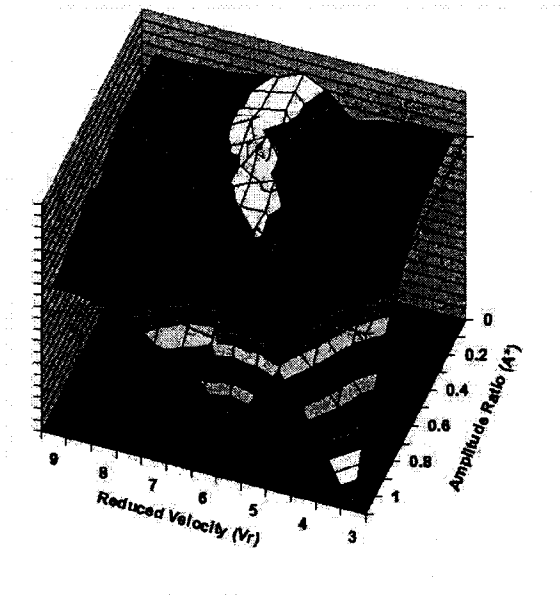


Figure 3-16: Lift Coefficient Plot

8. The magnitudes of drag force and lift force are computed for next cycle by

$$Drag = \frac{1}{2} \rho C_d U^2 L D$$

$$Lift = \frac{1}{2}\rho C_l U^2 LD$$

9. The VIV responses of the riser are obtained by repeating the Steps 2 to 8.

This procedure is only applicable to the VIV response with single mode. For multi-mode cases, another algorithm needs to be devised in the further research. The key parameters of the rigid riser were set the same as those in the experiments. The only difference is that the numerical model considers both inline VIV and cross-flow VIV, while only cross-flow VIV was considered in the experiment model. The numerical model of the rigid riser is shown in Figure 3-17. The key parameters are listed as follows

- Length: 6.02m
- Diameter: 0.325m
- Thickness: 0.01765m
- Stiffness of the support spring: 40000 N/m

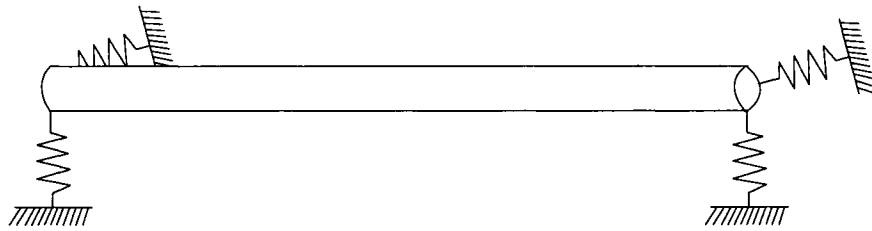


Figure 3-17: Rigid Riser Model

The VIV analyses were conducted for the riser at two current speed, 1.65m/s and 1.8m/s. The experimental database was used to interpolate the lift coefficients and validate the numerical results. The time series of cross-flow displacement are given in Figures 3-18 and 3-19. The nondimensional numerical solutions and the experimental

results are compared in Table 3.4. In Table 3.4, U is the current velocity, $U^* = \frac{U}{f_n D}$ is the normal reduced velocity, D is the outside diameter of the riser and f_n is the natural frequency of the riser. In the computation of U^* , the added mass coefficient, C_m , is given as 1. The numerical solutions by MAPS-Mooring agree well with the experimental data.

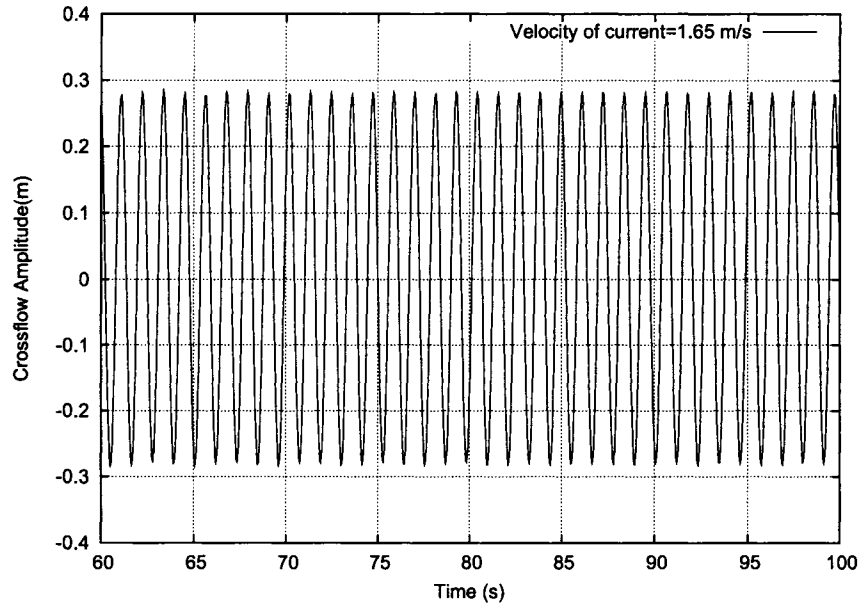


Figure 3-18: Cross-flow Motion of the Riser ($U=1.65\text{m/s}$)

Table 3.4: Comparison of Numerical Solutions and Experimental Results

U (m/s)	U^*	A^* (Experimental)	A^* (Numerical)
1.65	5.75	0.9	0.87
1.8	6.27	0.77	0.77

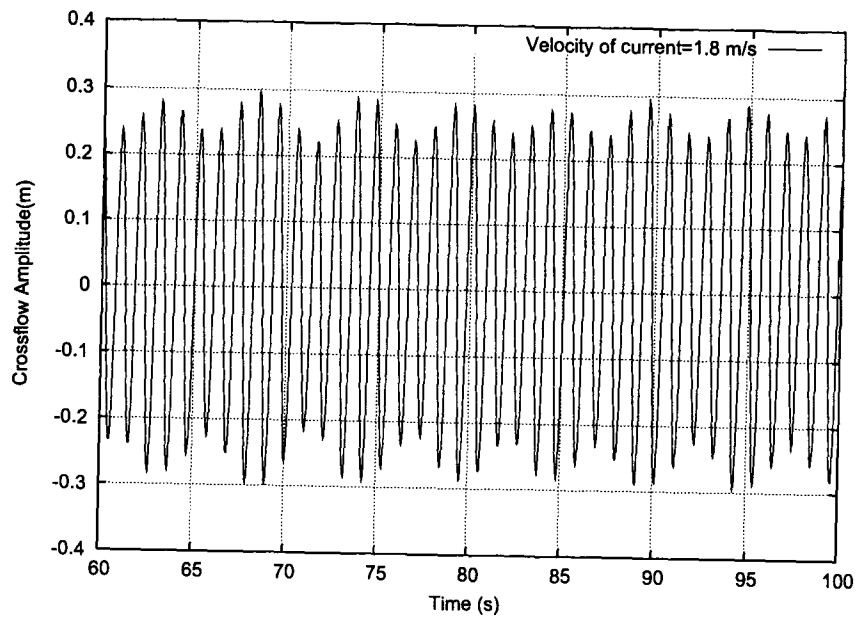


Figure 3-19: Cross-flow Motion of the Riser ($U=1.8\text{m/s}$)

Chapter 4

Conclusions and Recommendations

A numerical tool for the static and dynamic analysis of mooring lines and marine risers has been developed. The global-coordinate-based finite element method was used to model mooring lines and marine risers. In this method, the global coordinate system is used to describe the position of mooring lines instead of introducing local coordinate systems. The geometric nonlinearity and the environmental load nonlinearity are considered. Assuming that the sea bottom is flat and elastic, the sea bottom is modeled by an elastic layer (spring mat). The non-penetrating bottom boundary conditions are applied for both static and dynamic problems. Small elongation of the rod is considered in the equations of motion of mooring lines.

In the computation, the static problem is first solved to determine the initial profile of mooring lines. When solving the static problem, the inertia term is neglected. The governing differential equations of the mooring line are a set of nonlinear algebraic equations which are solved by Newton's iteration method. For dynamic problems, the second-order differential equations are substituted by a set of first-order differential equations. The first-order Adams-Moulton method is used to integrate the equations.

Base on the global-coordinate-based finite element method, a static and dynamic analysis program, MAPS-Mooring, has been developed. Validation studies have been carried out for both single mooring line and multiple mooring lines. Static and dy-

dynamic numerical results were compared with analytical solution, published numerical or experimental data. The accuracy and reliability of the developed program has been demonstrated in the validation studies.

The global-coordinate-based finite element method was also applied to simulate the vortex induced vibration (VIV) of a short marine riser in the time domain. The added mass coefficient, lifting force coefficient and drag force coefficient were calculated from the existing database, which was set up based on experimental results. The computed cross-flow displacements agree well with those from the model tests at two velocities of current. Further validation studies are needed for the short riser at a large range of current velocities. It is recommended to extend this method to flexible marine risers with multiple VIV modes.

References

- Ansari, K.A., 1986, "The Effect of Cable Dynamics on the Station-keeping response of a Moored Offshore Vessel," Proceedings of the Fifth International Offshore Mechanics and Arctic Engineering Symposium, Tokyo.
- Bathe, Klaus-Jurgen, 1996, Finite Element Procedures, Prentice Hall, Englewood Cliffs, New Jersey.
- Berteaux, H.O., 1976, Buoy Engineering, John Wiley & Sons, New York.
- Brown, D.T. and Lyons, G.J., 1998, Catenary Mooring Design Manual, Bentham Press, London.
- Chen, X.H., 2002, Studies on Dynamic Interaction Between Deep-water Floating Structures and Their Mooring/Tendon Systems, PhD thesis, Texas A&M University.
- Huang, S., 1994, "Dynamic Analysis of Three-dimensional Marine Cables," Ocean Engineering, Vol. 21, No. 6.
- Garrett, D.L., 1982, "Dynamic Analysis of Slender Rods," Proceedings of the 1st International Offshore Mechanics and Arctic Engineering Symposium, Dallas.
- Hwang, Y.L., 1986, "Nonlinear Dynamic Analysis of Mooring Lines," Proceedings of the Fifth International Offshore Mechanics and Arctic Engineering Symposium, Tokyo.
- Jain, R.K., 1980, "A Simple Method of Calculating the Equivalent Stiffness in Mooring Cables," Applied Ocean Research, Vol. 2, No. 3.
- Kamman, J.W. and Huston, R.L., 2001, "Multiple Dynamics Modeling of Variable Length Cable System," Multibody System Dynamics, Vol. 5.

Khan, N.U. and Ansari, K.A., 1986, "On the Dynamics of a Multicomponent Mooring Line," *Computers and Structures*, Vol. 22, No.3.

Kitney, N. and Brown, D.T., 2001, "Experimental Investigation of Mooring Line Loading Using Large and Small-scale Models," *Journal of Offshore Mechanics and Arctic Engineering*, Vol. 123, No. 1.

Lau, M. and Stanley, J., 2005, *SPREAD-MOORING: Software for Mooring System Load Analysis*, Institute for Ocean Technology, National Research Council of Canada.

Malahy, R.C., 1986, "A Nonlinear Finite Element Method for the Analysis of Offshore Pipelines, Risers and Cable Structures," *Proceedings of the Fifth International Offshore Mechanics and Arctic Engineering Symposium*, Tokyo.

Migliore, H.J. and Webster, R.L., 1979, "Current Methods for Analyzing Dynamic Cable Response," *Shock and Vibration Digest*, Vol. 11, No. 6.

Migliore, H.J. and Webster, R.L., 1982, "Current Methods for Analyzing Dynamic Cable Response 1979 to the Present," *Shock and Vibration Digest*, Vol. 14, No. 9.

Nakajima, T., 1986, "A New Three-dimensional Quasi-static Solution for the Multi-component Mooring Systems," *Proceedings of the Fifth International Offshore Mechanics and Arctic Engineering Symposium*, Tokyo.

Nordgren, R.P., 1974, "On Computation of the Motion of Elastic Rods," *Journal of Applied Mechanics*, *Transaction of ASME*, Vol. 41.

Patel, M.H. and Brown, D.T., 1994, "Catenary Mooring System," *Advanced Offshore Engineering*, Bentham Press, London.

Paulling, J.R. and Webster, W.C., 1986, "A Consistent, Large-amplitude Analysis of the Coupled Response of a TLP and Tendon System," *Proceedings of the Fifth*

- International Offshore Mechanics and Arctic Engineering Symposium, Tokyo.
- Ran, Z.H. and Kim, M.H., 1997, Nonlinear Coupled Response of a Tethered Spar Platform in Waves, *International Journal of Offshore and Polar Engineering*, Vol. 7, No. 2.
- Ran, Z.H., 2000, Coupled Dynamic Analysis of Floating Structures in Currents, PhD Thesis, Texas A&M University.
- Spencer, D., 2006, Oceanic Consulting Corporation, Private Communication.
- Triantafyllou, M.S., 1984, "Linear Dynamics of Cables and Chains," *The Shock and Vibration Digest*, Vol. 16, No. 3.
- Triantafyllou, M.S., 1987, "Dynamics of Cables and Chains," *The Shock and Vibration Digest*, Vol. 19, No. 12.
- Triantafyllou, M.S., 1991, "Dynamics of Cables, Towing Cables and Mooring Systems," *The Shock and Vibration Digest*, Vol. 23, No. 7.
- Triantafyllou, M.S., 1992, "Anchor Line Dynamics," *Hydrodynamics: Computers, Model Tests and Reality*, (Proceedings of Marin Workshops), Elsevier, Amsterdam.
- Wu, S. and Murray, J.J., 1993, 3-D Finite Element Analysis of Catenary Mooring, Part I - Finite Element Formulation, LM-1993-01, Institute for Marine Dynamics, National Research Council Canada.



